Characterizing the dynamics of EEG waveforms as the path through parameter space of a mean-field neuronal model: Application to epilepsy seizure evolution

Alejo J. Holgado-Nevado[a], Frank Marten[a], Mark P. Richardson[b], John R. Terry[a,b,c,d,*]

[a]*Faculty of Engineering, University of Bristol, Bristol, BS8 1TR, UK*
[b]*Institute of Psychiatry, King's College London, De Crespigny Park, London, SE5 8AF UK*
[c]*Department of Automatic Control and Systems Engineering, University of Sheffield, S10 2TN, UK*
[d]*Sheffield Institute for Translational Neuroscience, University of Sheffield, S10 2HQ, UK*

Abstract

In this paper we propose that the dynamic evolution of EEG activity during epileptic seizures may be characterized as a path through parameter space of a mean-field model, reflecting gradual changes in underlying physiological mechanisms. Previous theoretical studies have demonstrated boundaries in parameter space of the model corresponding to transitions in EEG waveforms between apparently normal, spike and wave and subsequently poly-spike and wave activity. In the present manuscript, we develop an evolutionary algorithm that can estimate parameters of an underlying model from clinical data recordings. Our method is novel in that rather than attempting to estimate parameters in the frequency domain, we instead estimate in the time domain, choosing parameters according to the best fit obtained between the model output and features of the observed EEG waveform. We present comparisons of such paths through parameter space from separate seizures from an individual subject, as well as between different subjects. We propose that this method provides a novel approach to classifying seizures and epilepsies in idiopathic generalized epilepsy on the basis of differences in seizure evolution characterized by the path through parameter space. We anticipate that such an explanatory approach to classifying epilepsies and seizures may have potential to provide biomarkers of treatment outcome that might be determinable at point of first diagnosis from routine clinical EEG.

Keywords: Neural mass model, Nonlinear parameter estimation, Genetic algorithm, time-domain estimation, bifurcation analysis, nonlinear dynamics

*Corresponding author
Email address: J.R.Terry@bristol.ac.uk (John R. Terry)

1. Introduction

The electroencephalogram (EEG) is a cost-effective, non-invasive technique for capturing information about macroscopic brain dynamics. Since its inception in the mid 1920s [5] it has become a common tool for studying brain activity, particularly in the clinical setting. The main reason for this, in addition to its non-invasive nature and cost, is the well documented relationship between dynamic waveforms of activity in EEG and the underlying brain state. In particular, conditions such as epilepsy, Parkinson's and schizophrenia are associated with pathological brain oscillations, which may manifest themselves within EEG activity (see [39] for a comprehensive review).

One of the challenges of relating the output of EEG to neurological disorders is a lack of understanding of the underlying generators of the dynamic waveforms recorded using EEG and the mechanisms responsible for transitions between apparently normal and pathological brain states. For this reason nonlinear differential equations are a natural candidate for exploring the generators of EEG (and Magnetoencephalography (MEG)) and there has recently been considerable activity developing models of macroscopic brain activity (see [11] or [9] for recent reviews). A further challenge is the likely patient-specific breakdowns in these generators or mechanisms, which limit the 'usefulness' of a general brain model. Consequently recent interest in this field has been focussed on developing techniques for extracting model "information" (e.g. parameters or equations) from EEG recordings [26, 46, 18].

Along these lines, in the current manuscript we introduce a novel framework for estimating the parameters of an underlying model such that the output of the model is matched to specific (user-determined) features of the temporal evolution of the EEG. The framework we describe is generic and can be usefully applied in any setting where there is a desire to fit a generative model to the dynamic features of macroscale neural recordings. Importantly it overcomes the issue of the complex bifurcation structures which nonlinear models typically exhibit and often confound more straightforward parameter estimators. Our motivation for developing this framework is a move toward patient-specific models of epilepsy that will ultimately be of use in the clinical setting.

Epilepsy is one of the most common serious primary brain diseases, with a worldwide prevalence approaching 1% [3]. Epilepsy carries with it significant costs, both financially (estimated at 15.5 billion euros in the EU in 2004, with a total cost per case between 2000 and 12000 euros [43]) and in terms of mortality (some 1000 deaths directly due to epilepsy per annum [38] in the UK alone). Further, the seemingly random nature of seizures means that it is a debilitating condition, resulting in significant reduction in quality of life for people with epilepsy.

Epilepsy is the consequence of a wide range of diseases and abnormalities of the brain. Although some underlying causes of epilepsy are readily identified (eg. brain tumour, cortical malformation), the majority of cases of epilepsy have no known cause [3]. Nonetheless, a number of recognised epilepsy syndromes have

been consistently described, based on a range of phenomena including age of onset, typical seizure types, and typical findings on investigation including EEG [42]. It has been assumed that specific epilepsy syndromes are associated with specific underlying pathophysiological defects.

Idiopathic generalized epilepsy (IGE) is a group of epilepsy disorders, including Childhood Absence Epilepsy (CAE), Juvenile Absence Epilepsy (JAE) and Juvenile Myoclonic Epilepsy (JME) which typically have their onset in children and young adolescents. Patients with IGE have no brain abnormalities visible on conventional clinical MRI and their neurological examination, neuropsychology and intellect are typically normal; consequently IGEs are assumed to have a strong genetic basis. At present clinical classification of IGE syndromes is based on easily observable clinical phenomena and qualitative EEG criteria (for example specific features of ictal spike and wave discharges seen on EEG); whilst a classification based on underlying neurobiology is not yet feasible. Developing a new classification of epilepsy based on underlying mechanisms is a key challenge and an area of very active current clinical endeavour [4].

A second key challenge in epilepsy is to find a more effective approach to treatment. Whilst the prognosis for patients with IGE is often assumed good, a large trial of antiepileptic drug (AED) treatment in recent-onset IGE and other unclassifiable generalized epilepsies showed that between a third and a half failed to achieve remission within 12 months using first-line AEDs [30]. For this large group of patients there is consequently an anxious period of time during which further seizures occur and additional AEDs are prescribed on what is largely a trial-and-error basis. Although comprehensive treatment guidelines for epilepsy exist [52], the evidence-base for treatment decisions, especially after treatment failure, is recognised to be relatively weak. Identifying markers of likely response to AEDs would revolutionise the approach to the management of people with epilepsy.

Epilepsy has often been referred to as a 'dynamic' disease [35], both in terms of its longer term evolution as a condition and for the manner in which brain activity evolves during a seizure. For example, in the case of CAE there is a classical "spike and wave" (SW) discharge at around 3Hz, which appears approximately synchronously across many channels of the EEG. For the purposes of clinical diagnosis, the presence of SW complexes in EEG is sufficient and has typically merited little further study. Indeed, studies of animal models of epilepsy [53] have suggested that the onset and offset of seizure is simply a random process. However, subsequent studies of seizure frequency and duration in human patients suggests that the concept of a purely random switch is incorrect [54] and closer inspection of clinical recordings from subjects with absence seizures shows that as the seizure develops, the recorded waveform evolves dynamically and often dramatically. For example, the amplitude of the spike may increase or decrease, additional spikes may appear - giving rise to so-called "poly-spike and wave" (PSW) complexes - and the wave and spike may interchange during the course of the seizure. Perhaps most significantly, seizure evolution over time is often similar when comparing recordings of different seizures from the same channel of the same subject, suggesting that the same underlying physiological mechanisms occur come into play each time (see Fig. 1). Epilepsies with

similar mechanisms of ictogenesis and similar treatment responsiveness presumably share abnormalities at the neuronal level which could be reflected in patterns of activity recorded in EEG.

The dynamic nature of EEG and of seizure evolution in particular, makes nonlinear differential equations a natural candidate to understand such phenomena and there has, in recent times, been considerable interest in modelling EEG phenomena, from the existence of alpha activity [27, 44] through to seizure states occurring in IGE [53, 45, 47, 7, 49, 31] and other epilepsies [57, 28]. Most recently in [32] we described two mechanisms for the transitions between apparently normal and seizure states, as well as the transitions observed during seizures (e.g. the addition of extra spikes as the absence seizure evolves). Using a combination of mathematical analysis and numerical continuation methods [48, 14], bifurcations (both real and false) were shown to explain the appearance of oscillatory activity in EEG and the appearance of spikes. These studies also highlighted how changes in different parameters (for example excitation and inhibition) could give rise to very similar seizure evolution when examining the macroscopic variable. It is this similarity in macroscale dynamics, resulting from fundamentally different underlying mechanisms, which could explain why clinical diagnosis based upon a cursory study of EEG results in non-specific treatment outcomes.

The method we develop is used to estimate parameters of the macroscopic brain model we studied in [32] and explores if these parameters evolve in a consistent manner during a seizure. The underlying hypothesis is that these aggregated parameters reflect underlying (but unidentified) physiological processes and that the onset, evolution and offset of seizures can be related to parameter shifts over time. We achieve this by developing a genetic algorithm that can estimate all model parameters in finite time and explore how these parameters vary during the course of a seizure. As described above, the method we propose differs significantly from previous attempts to estimate parameters from EEG in that we attempt to fit the specific *characteristics* of each cycle of the seizures, rather than attempting to estimate parameters by fitting to spectral features averaged over a longer period of time [46, 57]. We expect that reliable identification of parameter shifts over time through ictal discharges will motivate new hypotheses to explain the mechanisms of ictogenesis and seizure termination.

The remainder of the paper is arranged as follows. In section 2 we describe the background to the mathematical model, whose parameters we wish to estimate and describe the assumptions that we make to allow us to relate clinical recordings with the model output. Subsequently we describe the genetic algorithm that we use to obtain parameter estimates. In section 3 we present the results of the algorithm, comparing parameter estimates with random selections of parameters, before considering the results from three subjects, each having two seizures. In section 4 we discuss our findings, make suggestions for improving both model and algorithm and comment on the direction of future research.

2. Methods

2.1. A neural mass model for seizure EEG recordings

EEG is a technique used to record electrical activity from the surface area of the brain. This activity can be thought of as the summation of the interactions of large populations of cortical neurons, predominately cortical pyramidal cells, which receive both excitatory and inhibitory postsynaptic potentials and as an output generate extracellular currents. The summation of these currents occurs due to the alignment of the dendrites of pyramidal neurons - perpendicular to the scalp - whilst the activity within dendrites that are tangential are unmeasured.

Currently, attempts to interpret EEG signals using basic biophysical assumptions remains an active area of research. Some modellers choose to mimic the activity giving rise to EEG by simulating large scale neuronal networks, which have led to some valuable insights and predictions, see [8, 12, 24], for brain rhythms and neurological disorders. However, the complexity of these networks approaches typically precludes attempts at rigorous analysis of the mechanisms underpinning transitions in EEG waveforms observed experimentally. Hence, a natural question to consider is whether the complexity of these models can be reduced, enabling a simpler modelling approach to be considered?

During seizure activity, it has been shown that extensive brain networks fire in a synchronous manner [33]. In terms of the network models described previously, this implies that large populations of neurons form clusters in which they fire synchronously. Hence, a natural alternative to the network framework that is suitable to characterise this type of activity is provided by "neural mass" theory. The idea underpinning this theory is that rather than simulate the individual dynamics of a large population of neurons (neural masses), the aim is to simulate their average dynamics (i.e. firing rate or membrane potentials). The early development of this theory is based on pioneering phenomenological studies by Lopes da Silva [29] and Freeman [17], who were amongst the first to model neural population dynamics from experimental data. Around the same time, theoretical models were developed, including the seminal paper of Wilson and Cowan [58], who investigated oscillatory properties of coupled neural masses. Inspired by this study, researchers developed a spatially extended description designed to simulate two-dimensional sheets of cortical tissue, as in the works of Nunez [40], Amari [1] and more recently Jirsa & Haken [25].

As described in the introduction, from these early studies, the theory of neural masses has been used to characterise many different EEG phenomena (i.e. the alpha rhythm, sleep state and most importantly, for the purposes of the present study, different branches of epilepsy research. The specific mean-field model that we relate to EEG dynamics from idiopathic generalized epilpesies is based on the interaction between two brain regions, the thalamus and the cortex. Together they form a crucial component in generating spike wave rhythms [12, 13, 51] such as those observed in the recordings of Figure 1. The model consists of three connected neural masses [32], shown in Fig. 2(a). From top to bottom; a mass of cortical pyramidal neurons

(e), cells in the reticular thalamic nucleus (r) and specific thalamic neurons (s). Each mass is described by a variable $V_j(t)$, $j = e, r, s$, that represents the average post-synaptic potential (PSP) of each population. Following Freeman [17], the rate of change of $V_j(t)$ for each population can be modelled by the following differential equation:

$$\left(1 + \frac{1}{\alpha}\frac{d}{dt}\right)\left(1 + \frac{1}{\beta}\frac{d}{dt}\right)V_j(t) = \sum_{j'} \nu_{jj'}\phi_{j'}(t), \tag{1}$$

stating that $V_j(t)$ is driven by the linear weighted sum of all inputs from pre-synaptic neural masses j'. The time constants α and β are postsynaptic decay and rise times respectively. The connection weights $\nu_{jj'}$ determine the coupling strengths, along the arrows in in Fig. 2.

Axonal field variables $\phi_j(t)$ describe the signal propagation from one mass to the next. For cells in the thalamus, they are taken to be approximately equal to the firing-rates; $\phi_r(t) = F[V_r(t)]$ and $\phi_s(t) = F[V_s(t)]$ where

$$F[V_j] = \frac{Q_{max}}{1 + e^{-\frac{\pi}{\sqrt{3}}\frac{V_j - \theta}{\sigma}}} \tag{2}$$

describes the probability of firing for the neural masses. If the PSP-variable V_j is above threshold θ the mass fires action potentials at a rate $F[V_j]$. We have also included a sub-thalamic field $\phi_n(t)$ which can be used to model sensory input (for example by white noise [53]). In our present investigation this is kept fixed to a constant value.

Two additional features are necessary to close this model. First of all, the long range connectivity in cortical tissue is modelled by a wave-equation for the axonal field ϕ_e of pyramidal cells [25]. Because absence seizures display an almost synchronous EEG rhythm over the entire cortex, we only study spatially independent solutions of this equation, which satisfy:

$$\left(\frac{1}{\gamma_e^2}\frac{d^2}{dt^2} + \frac{2}{\gamma_e}\frac{d}{dt} + 1\right)\phi_e(t) = \nu_{ee}F[V_e(t)], \tag{3}$$

where γ_e is the inverse of the timescale over which cortical axonal fields spread out. Since ϕ_e represents the spread of activity in the cortex, this is the variable that we regard as being compared to EEG recordings (We provide further motivations for this choice, as well as alternative interpretations in the discussion section). Finally, the scheme in Fig. 2 displays two connections from (r) onto (s); one is simply $\phi_r(t) = F[V_r(t)]$, whereas the other is a field $\phi_B(t)$ of slow inhibition governed by GABA_B receptors (see [12, 32] for a detailed description). These differences in time-scales can be thoughts of as being due to the differences in receptor bindings (GABA_A being ionotropic, whereas GABA_B is metabotropic). It satisfies the following equation:

$$\left(1 + \frac{1}{A}\frac{d}{dt}\right)\left(1 + \frac{1}{B}\frac{d}{dt}\right)\phi_B(t) = F[V_r(t)], \tag{4}$$

where A, B are the inverse decay and rise times of the inhibitory potential caused by GABA_B.

In summary, our model is a nonlinear dynamical system comprising 5 variables ϕ_e, V_e, V_r, V_s, ϕ_B, each of which observes a second-order differential equation. In past studies [7, 31, 32] it was shown that these equations support 3Hz periodic solutions, which resemble spike-wave activity during absence seizures (see Fig. 5b1-b2). Note that we plotted $\phi_e(t)$ upside down; as clinical convention is to plot negative upwards, hence we also conform to this convention.

Two important issues arise when attempting to relate EEG dynamics during seizures to the output of a mean-field model. Firstly, as was already mentioned in our introduction, waveforms during spike and wave discharges (Fig. 1) do not show a "perfect" periodic rhythm. Rather their dynamics evolve as the seizure progresses, with spikes (dis)appearing and typically a slow decrease in frequency. Hence one cannot simply compare a periodic solution of the model to clinical data from the full spike and wave discharge. From the dynamical systems perspective, these EEG rhythms can be interpreted in 3 different ways (Fig. 3): The first case presented in panel (a) is that the evolution of EEG dynamics can be represented as a dynamic attractor, whose shape evolves (due to variations in underlying system parameters) as the seizure progresses. In such a scenario the attractor could either be a stable periodic solution or a chaotic state of the model. An alternative scenario, considered in panel (b) is that of a transient solution evolving around an attractor which does not change its shape. In this scenario there is no changes in underlying system dynamics per se. A final scenario, considered in panel (c) is a merging on the situation considered in panels (a) and (b), whereby EEG dynamics can be captured by a transient solution about a dynamic attractor. In this work we hypothesise that there is some form of dynamic attractor and that further, changes in the attractor occur slowly enough, that its true shape can be captured over a short time period. In the next section we shall consider this matter further.

Secondly, in our previous work [32] we demonstrated that the parameter-space of the model contains distinct regions with similar solutions for $\phi_e(t)$. See for example the dark red areas in Fig. 2(b); when placing model parameters in either of the two regions, the outcome is a 2-4Hz periodic solution with 3 spikes. Given the number of parameters of the model, it is likely that these types of behaviour will occur for other parameter choices as well. Consequently, when attempting to fit model output to data, we would expect to obtain several "local minima" of a chosen error function, giving rise to distinct parameter sets leading to very similar "model EEGs". To deal with this problem, we require an algorithm that takes distinct local minima into account. As we shall motivate in the following sections, genetic algorithms provide a natural framework for which to address this problem. To assist the reader with the description that follows we provide an overview of the entire process in Fig. 4.

2.2. Filtering methods for EEG and model output

A further challenge with relating experimental recordings to the output of the model, is that for any given model, only certain features of the data will be captured. Typical EEG recordings contain a high proportion of noise, which in this context we would include electrical activity generated by muscle function, blood flow and other phenomena not directly related with the firing rate of pyramidal neurons (For a discussion of these issues see chapter 59 of [39]). Since the model only considers the average activity of pyramidal neurons as the generator of the EEG signal and not any sources of additional noise, then prior to fitting the parameters of the model to the experimental data, it is necessary to eliminate (as best as possible) these sources of noise, hence preserving the part of the signal that can be reproduced by the chosen mathematical model.

To reduce the proportion of (high frequency) noise in the EEG recordings, we pay attention to two facts. First, the polyspike complexes generated during spike and wave discharges, contain two predominant frequencies - one of 2-4Hz corresponding to the slow wave, and another of 10-30Hz corresponding to the sudden spikes. Secondly, besides the aforementioned noise there are distinct > 30Hz components which form small sharp spikes in the signal; see for example the red circle markers in Fig. 5(a1). However, the chosen mathematical model can not reproduce such features. There are two approaches we can take as this juncture. One is to increase the complexity of the model, adding dynamical mechanisms that might enable the capturing of such additional features. Alternatively, we could decide that these features are not significant in describing the evolution of spike and wave discharges, relative to the other features which occur at consistent points throughout each seizure. In the present study, we follow this second option and apply a low-pass data filter which retains the prominent (less sharp) spikes, whilst removing both noise fluctuations and the small sharp spikes.

The simplest option to eliminate all frequency components above 30Hz, would be to calculate the fast Fourier transform of the EEG recordings, eliminate all components above 30Hz, and apply the inverse fast Fourier transform to the result. However, when trialling this technique on real data, the filter produced oscillations in the slow wave portion of the signal. To avoid this artefact, we use a smoother filter, namely the digital second order Butterworth method. See Figs. 5(a1)-(a2) for an application of this filter to our EEG data, which is timesampled at a rate of 169 Hz (these recordings being taken as a part of routine clinical practice). Note that it removes the small sharp spikes, whilst retaining the prominent data features.

Even though this filter does not remove the main features of our data, it can however be seen in Fig. 5 that the shapes of some spikes alter slightly as a result of the filtering process. Hence we reason that a similar (if not identical) filter should be applied to the "model EEG" variable ϕ_e, to bring data and model closer together. Instead of applying the same digital Butterworth filter used on the real data, we decided to take its analogue (continuous) counterpart for our model output. The reason for this is twofold:

- The model is a continuous dynamical system and a continuous Butterworth filter can simply be added

using two extra differential equations.

- It still allows the use of continuation methods for analysing bifurcations of the model, which we consider in the results section.

The two differential equations which define the continuous Butterworth filter are given by:

$$\begin{aligned} \frac{d\phi_{eF}(t)}{dt} &= u(t), \\ \frac{du(t)}{dt} &= \omega_c^2\Big(-\phi_{eF}(t) + \phi_e(t)\Big) - \sqrt{2}\cdot\omega_c\cdot u(t), \end{aligned} \tag{5}$$

which transform the variable $\phi_e(t)$ into a filtered variable $\phi_{eF}(t)$. The parameter $\omega_c \equiv 2\pi f_c$ defines the cutoff frequency f_c of the filter. As for the digital data filter, this is a second order Butterworth system. In both the model and the data filter we set $f_c = 30$Hz. For a qualitative comparison between data and model filter, see Fig. 5(c-d). Note that they are slightly different past the 3dB point at 30Hz, which is caused by the relatively low sampling rate (169Hz) of the clinical EEG recordings in our database. We will return to this issue in our discussion.

2.3. Segmentation of the spike and wave discharge into individual cycles

From an initial by sight examination of EEG recordings from our clinical database, we observed that independent of system noise, the dynamical features of the waveform evolve gradually from cycle to cycle throughout the discharge. As discussed in our modelling section, we hypothesise that the gradual change in the shape of these waves is due to slow variation in underlying system parameters of the neural system, whose pyramidal neurons generate the observed signal. At this stage, it is natural to consider the most appropriate manner with which to treat this continuous measure of EEG voltage, so as to allow us to elucidate any slow parameter variations in the model. Typical approaches to this problem have divided the entire data recordings to a finite number of periods - i.e. interictal, pre-onset, onset and ictal [57]. However this method has a number of shortcomings. First, it permits only a very low time resolution on the parameter evolution (i.e. only one datapoint that summarizes the entire duration of the discharge). Secondly, these types of approach usually only consider approximating the frequency spectrum of each of these sections. Only capturing the frequency properties of the signal, will typically not lead to a model output that replicates the prominent features of the EEG to which it is being fitted.

Given the consistency of evolution of the waveform across different seizures from the same subject, in particular the appearance of additional spikes at the almost identical timepoints in each (see Figure 1), suggests that capturing these features will be significant when characterising evolution across a seizure. Consequently, we consider an alternative approach, which is to divide the whole spike and wave discharge into individual near-periodic spike-wave cycles, the features of which we subsequently fit independently of

each other. This allows us to obtain a time resolution of the parameter evolution approximately an order of magnitude higher than with typical procedures. Given that the duration of spike and wave discharges is typically $\leq$ 10s [39], then our method provides up to 30 datapoints (assuming an approximate average frequency of 3Hz).

Due to the gradual change of wave shape, and to the complex form that polyspike cycles commonly have, no standard algorithms can be used to segment the denoised EEG signal into the independent cycles as we would desire. Therefore, we developed our own automated technique to perform the segmentation. The method is robust to noise, gradual wave shape variation, and slight variations in frequency across the time-series; all of which are prominent features of EEG recordings during spike and wave discharges.

The first step in our method is to establish the approximate period T of cycles within the particular recording, as this number can differ markedly (by up to 2Hz), from subject to subject. A mathematical integral can extract the information on the period of a signal, even if the signal is corrupted by a high proportion of noise. We call this integral function the periodicity function $p(\tau)$ of the denoised time-series $g_F(t)$. Although $p(\tau)$ can be also calculated for the original time-series (either EEG recording or model output) $g(t)$ (i.e. with noise), we prefer to calculate it on the denoised signal to further enhance robustness. The equation for $p(\tau)$ is given by:

$$p(\tau) = \lim_{n\to\infty} \frac{1}{2n} \int_{-n}^{n} \|g_F(t) - g_F(t+\tau)\|\, dt \tag{6}$$

which, in the case of a finite time-series, can be redefined as:

$$p(\tau) = \frac{1}{n} \sum_{t=0}^{n} \|g_F(t) - g_F(t+\tau)\| \tag{7}$$

where n is the number of sample points of our filtered signal $g_F(t)$. Depending on whether the considered time-series was fully denoised (i.e. the output of the model) or still contained some level of noise (i.e. the EEG recordings), the appearance of $p(\tau)$ will slightly change, as shown in Fig. 6. In both cases, the period of the signal will correspond with the smallest value of τ, for which all $p(k \cdot \tau)$ with $k \in \{1, 2, ...\}$ are local minima. The value of τ defined in this manner can be readily obtained with a simple computational algorithm, once the periodicity $p(\tau)$ function has been calculated.

Once the period T of the spike-wave discharge has been calculated, the final step is to filter the original signal with a thin pass band filter (the pass band lies between frequencies of 0.9 and 1.1 times 1/T). If such a thin filter is performed, a regular sinusoidal wave will be obtained, whose local minima can be used as cutting points for the original signal. These cutting points have properties that makes the procedure very appropriate for our purposes: their position is robust to noise, they can adapt to signals with a slowly varying frequency and cycle shape, and crucially are automatically calculated.

2.4. Extracting features from individual EEG cycles

The next step is to extract the crucial features of the data which we wish to replicate in the output of the model for an appropriate choice of system parameters. Each individual (poly)spike and wave cycle is made up of a number of key ingredients, namely, the spikes, the local minima between spikes (we refer to these as dips) and inflection points. Additionally the number, ordering and position each takes across a cycle may all be a reflection of changes in underlying physiological mechanisms controlling seizure evolution. If, for an individual cycle, we can identify the set of parameter values for which our model can produce "identical" features (i.e. the same number, ordering and position in the cycle) then this set of parameters most likely reflect the state of the underlying network. The simplest method to try to identify such a set of parameter values, would be to try to reproduce the values of the signal $g_F(t)$ at each point t (i.e. use a fitting algorithm based on the measure of squared error). However, this approach produces a very poor performance, and although the values of $g_F(t)$ can be relatively approximated, the key features are commonly missed. An alternative approach that we use to solve this problem, is to first extract the different qualitative features of each cycle, whose number, order and position will be later fitted by the algorithm (see section 2.5).

In the case of both real EEG and simulated data, the signal tends to contain either residual noise or artefacts which can be easily mistaken for a key feature of the cycle by simple feature detection algorithms. Conversely, algorithms which are more robust to this types of noise and artefacts, tend to require more computation time, and this can dramatically increase the total time of our search algorithm, rendering parameter estimation in real time impossible. Consequently, we designed a specific feature detection algorithm, which is robust to noise but executes in finite time (complexity $O(n)$).

This feature extraction algorithm is based on a finite state machine, whose Mealy definition can be found in Fig. 7(a). This machine follows the common rules of finite state machines, where the machine 'runs' by sequentially reading elements of a long array on a succession of time steps. In each time step, the machine is on one of a collection of possible states, which are represented in Fig. 7a by closed circles. To pass from the present time step to the next one, the machine 'reads' the following element on the input array, and depending on the value of such element, the machine changes from the present state to one of the other possible states (transition are represented by arrows). For each one of these transitions, the machine can also perform some operations, which are directly defined by which transition the machine made (in the diagram, the input which triggers a transition is written besides the operation that such a transition generates, in the standard *input/operation*).

In our case, the machine has five states: *INITIAL*, *UP*, *longUP*, *DOWN* and *longDOWN*. The input array is the discrete signal $g_F(t)$, which consequently will dictate all the state transition taking place on the machine. At time step 0, the machine is at state *INITIAL*. During the successive time steps, if the signal $g_F(t)$ is increasing (i.e. $g_F(t_i) < g_F(t_{i+1})$), the machine will tend to the states *UP* and *longUP*. Conversely, if it is decreasing (i.e. $g_F(t_i) < g_F(t_{i+1})$), it will tend to *DOWN* and *longDOWN*. The difference between

UP or *DOWN* and *longUP* or *longDOWN*, is that the machine only reaches a 'long' state, if the accumulated signal change since the last spike or dip (a value calculated in the variable 's'), is bigger than a given threshold (s_θ). When the machine reaches a local maxima or minima in a long state, it is marked as potential spike or dip in the variables 'u' and 'd', respectively.

However, such maxima or minima are not confirmed until later, once the machine detects that the amplitude of the local maxima or minima is higher than s_θ (when a spike or dip is confirmed, its position 'u' or 'd' are stored into the vectors 'U' or 'D', respectively). The machine achieves this behaviour by differentiating between the *UP-DOWN* states, and the long counterparts (*longUP* and *longDOWN*). While the states *UP* and *DOWN* indicate that $g_E(t)$ is respectively growing or decaying, *longUP* and *longDOWN* indicate that the next local maxima or minima may be an spike or dip, respectively, not an artifact of amplitude smaller than s_θ. However, such a possibility is not confirmed until the machine transits again into $longUP$ or $longDOWN$, respectively, which eliminates the possibility that local maxima and minima, of amplitude smaller than that s_θ, were mistaken by spikes or dips. Two examples of how the algorithm 'runs' on EEG with and without noise, can be seen in Fig. 7(b). As mentioned, this procedure executes quickly, and its feature detection capabilities are robust to noise and artefacts.

If this same finite state machine is applied to the derivative of $g_E(t)$, all the inflection points existing in $g_E(t)$ will appear as spikes or dips in the signal. However, there will be other spikes and dips in $\frac{dg_E(t)}{dt}$ which do not correspond to turning points in $g_E(t)$. The key feature of the inflection points of $g_E(t)$, is that they will generate spikes or dips only when $\frac{dg_E(t)}{dt}$ is near to 0. Therefore, the turning points of $g_E(t)$ can be easily obtained by calculating its derivative and running the finite state machine on this. All spikes and dips points found within a threshold of 0 can be considered as turning points.

2.5. Defining free parameters and an error function

Having successfully identified the features of an individual cycle, the next step is to find the parameter values of our mathematical model that reproduce the number, order and position of these features most accurately. To initialize this process, the following two steps must be undertaken. First, it should be decided which (if any) of the model parameters should be fixed to biologically plausible values (fixed parameters), and which should be estimated on the basis of the features of a segmented cycle (free parameters). Secondly, an heuristic error function must be defined, which assigns to each possible combination of free parameters an error value, which should indicate how accurately features of the model output (for the chosen parameter set) concur with those of the segmented cycle (i.e. if one combination of free parameter values has a lower error than another, this implies that the former choice produces model output that better replicates the features of the segmented cycle).

The first of these steps (i.e. to divide parameters into groups of either fixed or free) is by no means trivial. Due to the nature of mean-field models, it is difficult to relate biologically plausible values to which

one can fix parameters of the model. One approach to overcome this problem, is to classify all model parameters as free, and establish their values exclusively in the light of the experimental data contained in our clinical database. However, with 17 free parameters it quickly became apparent that the system was overparametrised, by which we mean that several choices of parameters generated equally accurate fits. An alternative approach that we utilise in the present work, is to fix most of the parameter values (using choices motivated by the study [46]), and allowing only a small subset to vary.

In the present study we decided to vary 3 parameters, one being purely cortical, one being purely thalamic, and one describing global dynamical behaviour of the thalamocortical loop. Their choice is based on a compromise between (1) finding a minimal set of parameters that allows us to model the (changes in) EEG features and (2) insights from past experimental and theoretical studies on IGE. The first free parameter is "γ_e"; it defines a ratio between signal propagation velocity in the cortex, and typical cortical length scales [25]. A number of recent experimental works [41, 6] suggest a focal onset region for absence seizures. Whilst our model does not support any spatial information (the cortex is taken uniform in Eq. 3), varying γ_E approximates the shift in cortical length scales (focus to generalized). The second free parameter is "A", the inverse decay time of inhibition governed by GABA_B receptors (Eq. 4). Various studies cited in [6] hypothesize that the gradual change of frequency in spike wave rhythms is caused by thalamic circuits. In our model, the slowest thalamic process (order 100ms) is captured by Eq. 4. Moreover, changing parameters of this equation alters the frequency of the 2-4Hz spike wave rhythms produced by the model. Similar to our past work [32] we fix the parameter ratio $B/A = 3$ to simplify the analysis.

A third parameter is required to ensure that the model can reproduce all features in Section 2.4. We decided to take "α". This parameter describes all synaptic connections in our model, apart from GABA_B, hence there is no plausible way to motivate it from literature. In addition we decided to fix the ration β/α to 3, which is an approximation to the values obtained from varying all 17 parameters. The specific choices of parameter values are given in Table 1, which we have used in our previous studies of the mechanisms underlying spike and wave discharges [32]. As alluded to above, the choice of free parameters is in some senses arbitrary and certainly difficult to justify biologically, hence we limit the results of our study to the case of classification of patients with IGE - i.e. the evolution of free parameters may not have an accurate biological interpretation, however different patterns of evolution could be used as a biomarker (see the Discussion for further information).

The second step is to design an error function which penalises choices of parameter values which poorly replicate the key features of a spike and wave cycle. Specifically, given a spike and wave cycle $g_{F,k}(t)$ and a cycle simulated from our model $g_{\vec{p}}(t)$ (which is the cycle generated by our model with free parameter vector

$\vec{p} = (\gamma_e, \alpha, A)$), the error function is denoted as $e\left(g_{F,k}, g_{\vec{p}}\right)$, and has the following form:

$$\begin{aligned} e &: \{\mathbb{R}^n, \mathbb{R}^m\} \to \mathbb{R} \\ e\left(g_{F,k}, g_{\vec{p}}\right) &= r_{k,\vec{p}} \end{aligned} \tag{8}$$

where n is the number of sample points of cycle k, m the number of simulation points in the simulated cycle, and $r_{k,\vec{p}}$ is the value of error given to the parameter values $\vec{p}$ for the simulated cycle compared with the seizure cycle k.

As a general description, the value of $r_{k,\vec{p}}$ depends on how similar are the number, order and position of the features of both cycles $g_{F,k}(t)$ and $g_{\vec{p}}(t)$. The element that most significantly influences the outcome, is a discrepancy in the number of features between both cycles, followed by their relative ordering inside the wave, while the relative position has the lowest influence. Similarly, the type of features that have most influence in such values are the spikes and dips, while inflection points have a lower influence. For these reasons, when considering a new combination of parameters $\vec{p}$ for a specific experimental cycle k, the algorithm will first try to reproduce the number of spikes and dips.

Once the algorithm has identified regions in parameter space which reproduce the appropriate number of features, the order of the positions becomes the major contributor to the value of the error $r_{k,\vec{p}}$. Consequently the focus of the algorithm shifts to matching the order of the number of features. Finally when the order of the features has been best approximated, the algorithm finally focusses on approximating the specific positions of each feature inside the cycle. Due to the complex bifurcation structure of our mathematical model, we found this error function to be a very suitable approach for reproducing each cycle of a spike and wave discharge. This was the case both when fitting three parameters, but also if more parameters (or all of them) are treated as free. The problem encountered with more free parameters is not the difficulty in reproduce a cycle, rather that this method finds too many combinations of parameters which approximate each experimental cycle.

2.6. The genetic algorithm

Once the error function has been defined, the final step to fit the output of our mathematical model to each one of the independent EEG cycles, is to design an automated search algorithm that finds the combination of free parameter values that minimizes the error function. Of the different options available, an advanced genetic algorithm appeared most appropriate. We concluded this primarily because it is commonly argued that genetic algorithms, although slow, are the best option within the field of artificial intelligence to find the global minima of a complex error function [15, 36, 37]. A further argument in favour of a genetic algorithm is that the strong nonlinearities within our model which result in the complex bifurcation structures will most likely act as a confounder to other approaches, for example variational methods such as generalized filtering [18]. Additionally, we term our algorithm an 'advanced' genetic algorithm, because

it includes several enhancements to a classical genetic algorithm, which increase its performance (at least for the purposes that we require). A diagram of the general operations and steps taken by our algorithm is shown in Figure 8, which we refer the reader to for reference during our subsequent description of the algorithm.

Genetic algorithms are based upon the process of natural selection and evolution, which after a large number of generations produces organisms that are optimally adapted to a complex habitat. In imitation of this natural process, a genetic algorithm goes through a number of iterations, commonly called generations. For each generation, a collection of chromosomes - which are different possible combinations of the free parameter values - are tested against the predesigned error function that has to be optimized (i.e. the global minima of that function has to be found). The best chromosomes are held into the population (i.e. the collection of chromosomes), while the others are replaced by new chromosomes, which are copies of the surviving ones. Finally, the algorithm performs some modifications and recombinations (mutations) of the parameter values stored in the chromosomes, which aim to create previously unexisting combinations of parameter values whilst maintaining the best current choices existing in the population. With this process a new population is created, and the previous steps are repeated on this new population. This therefore becomes an iterative process that is repeated until a sufficiently good chromosome is found (i.e. a combination of parameter values that reproduces the experimental data with sufficient accuracy).

The whole iterative process described in the previous paragraph, is known as the classical or canonical genetic algorithm. For some applications, more advanced features are added to this general algorithm, which aim to increase the performance or to specifically adapt the process to a particular objective. For our case, we added some advanced features: error sharing [10, 19], uniform [55] and arithmetic chromosome recombination [34], elitism [20] and stochastic universal sampling [2]. Apart from these, there are two other advanced features that are not commonly utilised in the field. One of them is an additional genetic operand, which performs a local hill climbing search with inertia [36] to generate a new chromosome from a preexisting one. The other is a simple but effective mechanism that we have called freezing. This mechanism counts the number of copies that have been made of each chromosome to generate new ones. Due to elitism, the best chromosomes will always remain in the population and, possibly, never be eliminated, generating in each generation new chromosomes similar to itself. However, if this good chromosome is situated in a local minima with a wide basin of attraction, it will possibly be incapable of generating new good chromosomes. However, because this is a good combination of parameter values, it will generate a high number of copies in each generation. The freezing mechanism detects such 'local minima' chromosomes and once the count of offspring have surpassed a threshold, they are eliminated from the main population and stored in a 'frozen' population. The chromosomes stored in this frozen population are treated in all respects as chromosomes of the main population, except for the fact that new chromosomes will not be created as copies of them. As shown in Figure 2(b), markedly different regions of the parameter space can have equivalent numbers of

features, as determined by the bifurcation structure. Consequently chromosomes could become trapped in one region of parameter space, which whilst having the correct number of features, their order and phase position may not be as accurate as for other regions of parameter space. The advanced operations we introduced are designed to overcome this issue.

This genetic algorithm is designed to find the best combination of parameter values to reproduce the shape of each one of the segmented waves (see subsection 2.3). However, due to stochastic sampling, the 'best' parameter choice by the genetic algorithm can differ from one execution to another. Therefore, it cannot be assumed that the algorithm will always find the best combination of parameter values for each segmented cycle. To improve the probability of finding the most appropriate combination of parameter values, we ran the described genetic algorithm multiple times per segmented cycle on a cluster of 4000 cores. This process produced a set of 440 combinations of parameter values per cycle.

2.7. Determining the path through parameter space

As described in the previous subsection, once the experimental EEG has been filtered, segmented into independent cycles, the features of each cycle extracted, and these features have been fitted numerous times, we obtain a collection of 440 fits (each one denoted as a parameter vector $\vec{p} = (\gamma_e, \alpha, A)$) for each cycle. Not all of these fits will represent the specific cycle equally well, given the stochastic nature of our genetic algorithm. For example, some fits will contain more (or less) spikes than the actual EEG. To reduce their effect on our parameter analysis, we decided to use the 20% of fits, with the lowest value of error function per cycle.

Ideally, these selected 88 fits per cycle will all appear concentrated around a unique point in parameter space, forming a cluster (see for example the lower left panel of Fig. 11(a)). However, due to the complex bifurcation structure of the model (see Fig. 2), frequently these fits will appear not around a single point, but will cluster around two or more (see Fig. 9). Therefore, an approach has to be established to determine for each cycle with more than one cluster of fits, which one should be chosen to represent the parameter values of that cycle. From the perspective of the algorithm, the reason that a cycle can show multiple fit clusters, is that the error function $e\left(g_{F,k}, g_{\vec{p}}\right)$ contains more than one local minimum in the vector space P (defined as the vector space in $\mathbb{R}^3$ which contain all the possible combinations of free parameter values (γ_e, α, A)).

The first step to deal with this problem is, to identify the number of clusters of a particular cycle. For this we use the Matlab function "subclust" with default settings. We illustrate its outcome, for an exemplar spike-wave discharge, in Fig. 9. It must be emphasized that the clustering is performed in the full three dimensional parameter space, and this figure shows the cluster centers projected into one parameter. To illustrate the multi-cluster behaviour per cycle, see for example cycles 9 or 10 which contain two clearly distinguishable clusters. The second step consists of deciding which cluster 'best' represents the particular

cycle. We use the outcome of the "SUBCLUST" function to obtain cluster radii, count the number of members within each radius, and compute their average error function value. The best cluster consists of the one with the lowest average error. We believe that the center of this cluster is a good representative fit.

However, in some cases, we can not discount that for any specific experimental cycle $g_{F,k}(t)$ the approach may not select the best center. Whilst it is not possible in general to determine the suitability of any given choice, our hypothesis that we expect system parameters to evolve relatively smoothly during a spike and wave discharge, provides some clues. In particular, we would not expect centers from one cycle to the next to jump wildly in parameter space. Cluster centers that differ significantly from the trend of neighbouring cycles, when projected into any of the three parameters, are termed outliers. See for example the red cluster center in cycle 6 of Fig. 9. A further mechanism should be designed to counteract the effect of the outliers in the parameter evolution.

Additionally, there is another potential source of error, which stems from the very nature of our clinical recordings. Whilst, the filtering techniques described in subsection 2.2, does not tend to destroy the major qualitative features of each segmented cycle, the low sampling rate of the clinical recordings means that noise can on occasions eliminate one of the features (see Fig. 10). If we compare the sampling rate ($\sim$0.006 seconds) with the common period of spikes, dips and inflection points ($\sim$0.06 seconds), this phenomena, although infrequently, may occur in some of the sampled waves (e.g. if four consecutive time-samples containing a measurement error). This phenomena will also generate some outliers in the parameter estimates for each cycle.

The solution we adopt for the problem of outliers, is similar to the one used to eliminate noise in the original EEG recordings, only this time applied to the parameter estimates. As described above, the common characteristic of outliers is the difference in their values relative to those of neighbouring cycles. Further, by definition, we should expect the presence of outliers only infrequently across all approximated cycles (see Fig. 9). Therefore, we apply a smoothing technique which puts emphasis on past cycles, and suppresses rapid paramater fluctuations that do not follow the previous trend. A relatively simple method which accomplishes this, is exponential smoothing:

$$\begin{aligned} \vec{S}_1 &= \vec{p}_1, \\ \vec{S}_k &= \lambda \vec{p}_k + (1-\lambda)\vec{S}_{k-1}, \quad k = 2, 3, 4, ... \end{aligned} \tag{9}$$

where $\vec{p}_k$ is the parameter vector (γ_e, α, A) of the best cluster center of cycle k, and $\vec{S}_k$ is the corresponding smoothed parameter vector. The scalar constant λ, which is defined between 0 and 1, determines the degree of smoothing. Lower values of this constant indicate a higher emphasis on past observations. In our analysis, we used $\lambda = 0.3$ throughout. The resulting values of $\vec{S}_k$ define the path in parameter space, of a full spike-wave discharge. An illustration of this path, projected into parameter γ_e, is shown as the solid red curve in

Fig. 9. We will discuss more examples in section 3.

3. Results

3.1. Testing and validation using pseudo-data

Before attempting to characterise clinical recordings, we first tested the ability of the algorithm to reproduce parameter values, by fitting the model to itself. We produced simulated EEG from a random combination of parameter values, known from our previous bifurcation studies of the model to produce periodic (poly)spike waveforms. For a known parameter value, we produced three waveforms - each consisting of three cycles of oscillation. In particular, one waveform is noise free, one contains 2% white noise, and a third one contains 5% white noise, where the percentage indicates the standard deviation of the noise with respect to the amplitude of the waveform. In keeping with our real data, we downsample each simulated signal, to mimic the sampling frequency (5.6ms) of the clinical recordings. Finally, we use the fits of the middle (second cycle) of each waveform, and compare them to the original parameters that were used to generate simulation.

Specifically, the comparison is performed by selecting the 20% fits out of 440, with lowest error, cluster them and compute the cluster center with lowest mean error (the method details are given in subsection 2.7). A first example is shown in Fig. 11(a), where we used the parameter values $\gamma_e = 110, \alpha = 60, A = 16.4$ to generate a periodic single-spike waveform. The upper panels of the figure illustrate the second cycle of this waveform (black curves) and an exemplar fit of the model to this cycle (grey curve). For 0% noise we found the representative cluster center at $\gamma_e = 118, \alpha = 63.1, A = 16.6$. Increasing the noise to 2% gives a representative cluster center at $\gamma_e = 121, \alpha = 64.5, A = 17.0$. Finally, a noise level of 5% produces a center at $\gamma_e = 114, \alpha = 60.9, A = 15.6$. A good agreement for each noise level, considering that the parameters were allowed to vary on an interval of $[10, 200]$ for γ_e and α, and an interval of $[0.1, 100]$ for A.

Having obtained a good agreement between the random selection of parameter values and those obtained using our algorithm, we then proceeded to mimic a spike-wave discharge. We simulated twelve spike-wave cycles, each one originating from a different choice of parameters. Whilst belonging to independent simulations, the parameters of every cycle are chosen to be relatively close to the previous one, reflecting our assumption that a real seizure develops gradually with a slow change of underlying mechanisms. As with the case of the individual waveforms considered previously, we downsampled the cycles and added noise in the same proportion. The whole algorithm was then used to evaluate the path through parameter space, which was in turn compared with the (also smoothed) parameter path used to generate the 12 cycles. Figure 11(b) presents a comparison of the actual smoothed path through parameter space with the path estimated by the algorithm. There is again a good agreement between the estimation and the original parameter values chosen to simulate the seizure. This preliminary tests verify that the algorithm is capable of estimating

model parameters based upon key features of each spike-wave cycle. For the rest of this section, we consider results obtained using clinical EEG recordings.

3.2. Relating parameter clusters to model bifurcations

We now consider how the "clouds" of parameters for each fitted spike wave cycle $g_{F,k}$, that lie in the parameter space (γ_e,α,A) relate to the bifurcation structure of our underlying model. Given the features we selected for model-data comparison (section 2.4), we saw in the methods section how such regions will correspond to a particular spike-wave morphology in the model variable ϕ_{eF}. We now proceed using numerical bifurcation tools to obtain a better understanding of the relationship between our parameter clusters for successive spike-wave cycles.

A challenge that we must first overcome relates to the nature of numerical software packages for bifurcation analysis. Typically these packages allow for variation in at most two model parameters, whereas we are typically considering variation of at least three parameters (and potentially more). Interestingly when studying the parameters of all fitted spike-wave cycles we considered (3 patients, 2 spike wave discharges per patient, 88 fits per cycle), we observe that a majority appear to line up within a two-dimensional structure (see Fig. 12(a)). Using principal components analysis, we found that the 1st and 3rd component span a plane which captures most of this two dimensional structure (see coloured plane in Fig. 12(a)). Through an appropriate parametrization of this plane, we use the bifurcation package MATCONT [14] to investigate the spike-wave solutions of the model, limited to this plane.

In terms of model parameters, the two-dimensional plane is given by: $A = c_1 \cdot \gamma_e + c_2 \cdot \alpha + c_3$, where the constants $c_{1,2,3}$ follow from principal components . Hence the value of parameter A is now directly determined by γ_e and α. We thus use the latter two parameters as input for the bifurcation software; with the result of our analysis shown in Fig. 12(b). Note that there exist distinct regions in which the model produces 2-4 Hz periodic solutions (red shaded regions) and high frequency oscillations of 10Hz or more (blue shaded region). In addition, some parameters merely give rise to constant output without any oscillations (green region). The blue curves in this plane represent bifurcations (mainly limit points of cycles) on which the periodic solutions lose stability. For the purposes of this paper, we do not discuss the mathematical nature of these bifurcations, rather consider them as a means for explaining why different types of model solutions occupy particular regions of parameter space.

Within the 2-4Hz region of Fig. 12(b) we computed so-called false bifurcations as inflection points of the model (see [48]), shown as solid black lines. These divide the parameter space into regions within which the model variable $\phi_{eF}(t)$ displays periodic spike-wave oscillations with different numbers of spikes (see the pink to dark red shades in the legend). We can use this knowledge to better understand the parameter estimates that are produced by the algorithm. Figure 12(c,d) shows an example of two specific spike-wave cycles taken from our clinical database. The first cycle (panel (c1), black trace) features a single predominant

spike. The 88 fits of our model to this cycle, projected onto the bifurcation plane, are shown in panel (d1). The parameter cloud reveals that the genetic algorithm fitted single-spike solutions (leading to an elongated cloud, spanning most of the bifurcation region between $\gamma_e = 70$ and $\gamma_e = 200$). The second cycle (panel (c2), black trace) is a polyspike wave with two predominant spikes. The parameter clouds in panel (d2) show that the algorithm attempted to fit model solutions with two spikes. Because there are two distinct bifurcation regions which contain such solutions (see legend), the outcome are two distinct parameter clouds, one located in each region.

3.3. Application to patient data

We proceed to use the algorithm to characterize seizure evolution as the path through parameter space of the chosen parameters: γ_e, A and α, for three patients from our clinical database. It should be emphasized once more that γ_e is a purely cortical parameter (representing a ratio between signal propagation velocity and cortical length scales), A is purely thalamic (capturing a slow rhythm within the thalamus that could influence "wave" component of spike-wave discharges), and α is a global synaptic parameter of the entire thalamocortical loop.

The particular patients were chosen due to their having multiple seizure recordings, with seizure lengths in excess of four seconds, with low levels of observable noise across each recording. In addition to clinical recordings (typically taken at a first-referral clinic the database contains follow-up information, including antiepileptic drugs prescribed for each patient, as well as information about drug response (e.g. whether patients reported seizure free for 12 months following uptake of a particular AED).

For each patient (denoted A, B or C), we calculated the path through parameter space for two separate seizures, using the method in section 2.7. An exemplar of the model output in comparison to the actual clinical EEG is presented in Fig. 13. Significantly, we observe consistent trends in the calculated path for each patient. In the case of patient A (considered in Figure 14(a)) it can be seen that Seizure 1 commences with high value of α and evolves to lower values. Seizure 2 starts with a lower value in α, but starts following the same trend after cycle 4. A reason for this discrepancy is the presence of fast spikes in the first 0.6 seconds of EEG recordings, in Seizure 2. Our algorithm treated them as if they were spike wave cycles, leading to different parameter values in the first few cycles. The parameter A remains more consistent in each seizure, given that its values were allowed to vary on an interval of [0.1,100].

For patient B (considered in Figure 14(b)), a similar trend is apparent - albeit for different values of the parameters γ_e and α. In this case a trend downwards from the beginning of the seizure is apparent, with an increase towards the end. It is important to note the markedly different seizure lengths for this patient, reflected by the different length of the paths through parameter space (15 cycles for one seizure, versus 30 for the other). It is also important to note that the beginning values of γ_e and α are close to half those for patient A. Interestingly, near the ending of the shorter seizure, we observe that parameter γ_e departs

most from the common trend. Given our model, this would suggest a cortical role in seizure termination. However, such predictions should be verified with more biophysical models. The trend for parameter A is also similar again.

In the case of patient C (considered in Figure 14(c)), a different path through parameter space is observed. In this case an initial downward trend in parameter γ_e, in parallel with an increase in α is observed. Again the two seizures of this patient had different durations, leading to spike-wave discharges with very different numbers of cycles. We also note that near the ending of the shorter seizure, parameter α seems to depart most from the common trend. Hinting that this seizure may have a more global thalamocortical involvement that comes into play near its termination. Again, given our fairly arbitrary choice of parameters, such predictions should be verified using more biophysical models. Lastly, we note that the trends of patients A and C seem to take up similar regions in parameter space, as opposed to the trend in patient B.

Following these observations, we returned to the clinical meta-data associated with each patient. It is important to note that we were blinded to this information until after analysis of the parameter evolution. Interestingly, patients A and B, who displayed an initial decrease in α, were both diagnosed with CAE. However, whilst patient A responded well to medication, patient B did not. On the other hand patient C, for whom the path through parameter space exhibited an initial increase in α, was diagnosed with JME and did not respond well to medication. From this limited study, we can speculate that the overall trend of the path through parameter space may relate to diagnosis of seizure type, whilst the region of parameter space within which the evolution occurs, may relate to treatment response. Again validation of these observations require a more in-depth study in a large scale clinical database.

4. Discussion

In this paper we have described an algorithm that is capable of estimating parameters of a generative model from EEG data. In contrast to traditional methods of parameter estimation, which typically attempt to match model and data outputs in the frequency domain, we have developed a technique that can estimate parameters based on key features of the clinical data in the time-domain. We believe that this represents a significant methodological advance, since time-varying properties of the data are typically lost when considering only the spectral properties of the data. Our study was motivated by the observation that during spike-wave discharges from patients with idiopathic generalized epilepsies, the profile of the clinical waveform is not constant, but evolves dynamically during the discharge. We hypothesise that these changes in EEG are a reflection of variations in underlying mechanisms responsible for seizure onset, evolution and offset. Consequently, the ability to track changes in such mechanisms could significantly enhance our understanding of the condition.

To investigate this hypothesis we plotted the path through parameter space, taken as the value of chosen model parameters estimated from each spike-wave cycle during a discharge. For each considered patient, we

observed significant consistency in parameter evolution for independent seizures. Intriguingly, overall trends in parameter evolution observed across different patients, were consistent with diagnosis, but the region of parameter space within which the evolution occurred was markedly different. This observation suggests that spike-wave discharges in patients with idiopathic generalized epilepsies may not be randomly occurring events, but result from a number of different underlying physiological mechanisms, which are reflected in the EEG recordings. Probing these observations further will require a follow-up study in a large-scale clinical database, where the relationship between diagnosis and prognosis can be more systematically investigated. Longer term goals of this research would be to provide a methodological underpinning of clinical diagnosis of epilepsy and more significantly the ability to predict appropriate medication based upon EEG recordings made at a first-referral clinic. This second goal is particularly important, since there is increasing evidence that there is a significant correlation between the number of seizures a patient experiences and the likelihood of remission [21].

The patterns of parameter evolution revealed by our method may provide an objective and entirely novel approach to evaluating EEG in clinical practice. EEG reviewing and reporting in clinical practice is almost entirely subjective and dependent on expert interpretation. Such interpretation is heavily dependent on the identification of characteristic morphologic patterns of ictal discharge [56]. Recent clinical investigations have systematically described the qualitative features of generalised spike-wave bursts in absence seizures [50], but this attempt did not rest on any model of underlying mechanisms or dynamics, and provided only a summary of the changing EEG morphology through the ictal burst. Although this approach confirmed the diversity of ictal patterns in patients with similar syndromes, experience shows that expert EEG inspection may fail to reveal differences between patients who are syndromically different (see for example [59]). Our method holds promise to detect differences between patients which can be objectively described in terms of system dynamics, and hence may provide a more reliable description of EEG than expert interpretation alone. If it proves possible to predict prognosis (for example, time to remission from epilepsy) or response to treatment, this would be a major advance.

4.1. Methodological development

Whilst our preliminary results are promising, there are a number of important questions raised by our work that warrant further consideration. The first concerns the choice of model and beyond that the particular choice of free model parameters to be estimated by our algorithm. This is a natural question to ask and the answer is two-fold. Our choice of model was motivated by our previous mathematical studies [47, 49, 31, 32], which explored the underlying mechanisms responsible for the onset of (poly)spike-wave complexes in the model and demonstrated excellent agreement between model output and clinical recordings. It was these features, in particular the appearance and disappearance of extra spikes during a spike-wave discharge, that we felt were crucial to understanding seizure evolution and this reason underpinned our choice of model.

This choice highlights a more general consideration, namely that an understanding of the features of the clinical recordings believed to be important is crucial in informing the choice of model. Regarding the choice of parameters, this is somewhat arbitrary. One of the issues with the model we selected is that allowing all 17 model parameters to vary, results in an overparametrization of the system, whereby no clouds of best fits can form, due to the many optimal parameter choices. Consequently a subset of parameters were chosen so that we could appropriately characterise the shape (number of spikes), phase (ordering of the features) and frequency of each spike-wave cycle. The chosen subset could also be motivated by physiological considerations; for example a belief that particular mechanisms might vary during the course of a seizure would determine an appropriate subset of model parameters.

A further consideration with the chosen mean-field model is the lack of direct physiological interpretation of a number of system parameters. Firstly, this makes it difficult to determine the most appropriate set of values with which to initially fix model parameters. Secondly, it presents difficulties in providing a physiological interpretation of the path through parameter space. However, a systems level interpretation, for example relating diagnosis and prognosis to the path through parameter space is still possible using this framework. Finally, because the state variables of the mean field model have not a direct measurable interpretation, the amplitude and average voltage of an individual spike-wave cycle cannot be incorporated into the fitting process. We observe, in real EEG recordings that the amplitude and mean potential of successive cycles changes gradually during the seizure, and this change tends to be consistent within different seizures for an individual patient. However, a limitation of the considered mean-field model is that only the shape, phase and frequency can be interpreted. That said, understanding regions of parameter space for which particular waveforms are possible using bifurcation analysis, may enable a constraint to be placed on the search space. In this scenario, the regions of parameter space searched by the genetic algorithm, evolve iteratively according to regions of parameter space identified by bifurcation analysis has having the right features relative to the observed spike-wave cycle.

A practical consideration for model choice is the time taken to produce model output that can be compared to the clinical recordings. Due to the complex nonlinear nature of the model, it requires an advanced numerical solver with a small time-step to produce reliable simulations; requiring approximately 300 iterations per spike-wave cycle. This problem could be overcome by use of an alternative model, for example a firing-rate model such as that considered in [22].

Another question relates to our choice of electrode with which to compare model output and clinical recordings. Our choice of an occipital electrode was motivated by the fact, that this gave the most consistent, visually 'noise free', recordings across all of the patient data considered. Moving forward, using a combination of electrodes may represent the most appropriate means to characterize seizure evolution within the framework we have discussed. First of all, because recent experimental findings [23] suggest that certain generalized spike wave seizures are actually focal (starting in an isolated cortical region). Secondly,

because techniques exist to map a model with several cortical modules (each described by a neural mass of pyramidal cells) to an array of multiple EEG electrodes. See for example the 'lead field' methods discussed in [16]. Related to this, it would be desirable to have an increased sampling frequency of recordings, as a spike is of the order $50ms$, meaning that it is captured by only a few samples with the available clinical sampling rate of $\sim$ 170Hz. Sampling in excess of 500Hz would make it less likely to lose a crucial feature, such as a spike, due to the presence of measurement noise.

We conclude by noting that the framework we have developed here is highly generic. Whilst we have developed the framework with epilepsy in mind, the path through parameter space may be a useful tool for characterising a wide variety of evolving brain states that are observed using EEG recordings. Obvious examples include measuring the depth of anaesthesia [28], sleep state [13] and the potential to track the progression of neurodegenerative conditions such as Parkinson's [22], dementia and motor neuron disease. In all these cases, systems level dynamics will in part be a reflection of changes in underlying physiological mechanisms, and through the appropriate choice of model and feature extraction from data, elucidation of key mechanisms underlying these conditions may be possible.

5. Acknowledgments

FM, MPR and JRT acknowledge funding from the EPSRC via Grants EP/D068436/1"Mean-field modelling of human EEG: Application to Epilepsy Seizure Prediction" and EP/E032249/1 "Applied Nonlinear Mathematics: Making it real". JRT and MPR acknowledge funding from the MRC via grant G0701050 "Seizure prevention via control of neuronal activity". AJHN was fully funded by Caja Madrid Foundation, Madrid, Spain.

References

[1] Amari, S., 1975. Homogeneous nets of neuron-like elements. Biol. Cybern. **17**, 211–220.

[2] Baker J.E., 1987. Reducing bias and inefficiency in the selection algorithm. Proceedings of the Second International Conference on Genetic algorithms and their application.

[3] Banerjee N. M., Filipi D., Hauser W. A., 2009. The descriptive epidemiology of epilepsy - a review. Epilepsy Res. **85**, 31–45.

[4] Berg A. T., Berkovic S. F., Brodie M. J., Buchhalter J., Cross J. H., van Emde Boas W., Engel J., French J., Glauser T. A., Mathern G. W., Moshé S. L., Nordli D., Plouin P., Scheffer I. E., 2010. Revised terminology and concepts for organization of seizures and epilepsies: report of the ILAE Commission on Classification and Terminology, 2005-2009. Epilepsia **51** 676–685.

[5] Berger H., 1929. Über das Elektrenkephalogramm des Menschen. Arch. Psychiatr. Nervenkr. **87**, 527–570.

[6] Bosnyakova, D., Gabova, A., Zharikova, A., Gnezditski, V., Kuznetsova, G., van Luijtelaar, G., 2007. Some peculiarities of time-frequency dynamics of spike-wave discharges in humans and rats. Clin. Neurophysiol. **118**, 1736–1743.

[7] Breakspear, M., Roberts, J.A., Terry, J.R., Rodrigues, S., Mahant, N., Robinson, P.A., 2006. A unifying explanation of primary generalized seizures through nonlinear modeling and bifurcation analysis. Cereb. Cortex **16**, 1296–1313.

[8] Brunel, N., Wang, X., 2003. What determines the frequency of fast network oscillations with irregular neural discharges? I. Synaptic dynamics and excitation-inhibition balance. J. Neurophysiol. **90**, 415–430.

[9] Coombes S., 2010. Large-scale neural dynamics: Simple and complex. Neuroimage **52**, 731–739.

[10] Deb K., Goldberg D.E., 1989. An investigation of niche and species formation in genetic function optimization. Proc. Third Int. Conf. on Genetic Algorithms.

[11] Deco G. R., Jirsa V. K., Robinson P. A., Breakspear M., Friston K. J., 2008. The dynamic brain: from spiking neurons to neural masses and cortical fields. PLoS Comput. Biol. **4**, e1000092.

[12] Destexhe, A., 1998. Spike-and-wave oscillations based on the properties of GABAB receptors. J. Neurosci. **18**, 9099–9111.

[13] Destexhe, A., Sejnowski, T.J., 2001. Thalamocortical assemblies. Oxford University Press.

[14] Dhooge, A., Govaerts, W., Kuznetsov, Yu.A., 2003. MATCONT: A MATLAB package for numerical bifurcation analysis of ODEs. ACM Trans. Math. Softw. **29**, 141–164.

[15] Eiben, A.E., Smith, J.E., 2003. Introduction to evolutionary computing. Springer.

[16] Fastenrath, M., Friston, K.J., Kiebel, S.J. 2009. Dynamic causal modelling for M/EEG: Spatial and temporal symmetry constraints. NeuroImage. **44**, 154–163.

[17] Freeman, W.J., 1975. Mass Action in the Nervous System. Academic Press.

[18] Friston K., Stephan K., Li B. and Daunizeau J., 2010. Generalized Filtering. Math. Prob. Eng. doi:10.1155/2010/621670.

[19] Goldberg D.E., Richardson J., 1987. Genetic algorithms with sharing for multimodal function optimization. Proc. Second Int. Conf. on Genetic Algorithms.

[20] Günter R., 1994. Convergence Analysis of Canonical Genetic Algorithms. IEEE Transactions on Neural Networks **5**, 96–101.

[21] Hixson J. D., 2010. Stopping Antiepileptic Drugs: When and Why? Current Treatment Options in Neurology **12**, 434–442.

[22] Holgado-Nevado A. J., Terry J. R., Bogacz R., 2010. Conditions for the generation of beta oscillations in the subthalamic nucleus-globus pallidus network. J. Neurosci. **30**, 12340–12352.

[23] Holmes, M.D., 2008. Dense array EEG: Methodology and new hypothesis on epilepsy syndromes. Epilepsia. **49**(Suppl. 3), 3–14.

[24] Izhikevich, E.M., Edelman, G.M., 2008. Large-Scale model of mammalian thalamocortical systems. PNAS **105**, 3593–3598.

[25] Jirsa, V.K., Haken, H., 1996. Field theory of electromagnetic brain activity. Phys. Rev. Lett. **77**, 960–963.

[26] Jirsa V. K., Jantzen K., Fuchs A., Kelso J. A. S., 2002. Spatiotemporal forward solution of the EEG and MEG using network modeling. Medical Imaging, IEEE Transactions on **21**, 493–504.

[27] Liley, D.T.J., Cadush, P.J., Dafilis, M.P., 2002. A spatially continuous mean field theory of electrocortical activity. Network: Comput. Neural Syst. **13**, 67–113.

[28] Liley, D.T.J., Bojak, I., 2005. Understanding the transition to seizure by modeling the epileptiform activity of general anesthetic agents. J. Clin. Neurophysiol. **22**, 300–313.

[29] Lopes da Silva, F.H., Hoeks, A., Smits H. and Zetterberg, L. H., 1974. Model of brain rhythmic activity. Kybernetic **15**, 27–37.

[30] Marson A., Jacoby A., Johnson A., Kim L., Gamble C., Chadwick D., 2005. Immediate versus deferred antiepileptic drug treatment for early epilepsy and single seizures: a randomised controlled trial. Lancet **365**, 2007–2013.

[31] Marten, F., Rodrigues, S., Benjamin, O., Richardson, M.P. and Terry, J.R., 2009. Onset of polyspike complexes in a mean-field model of human electroencephalograph and its application to absence epilepsy. Philos. Trans. Royal Soc. A **367**, 1145-1161.

[32] Marten, F., Rodrigues, S., Suffczynski, P., Richardson, M.P., Terry, J.R., 2009. Derivation and analysis of an ordinary differential equation mean-field model for studying clinically recorded epilepsy dynamics. Phys. Rev. E **79**, 021911.

[33] McCormick, D.A., Contreras, D., 2001. On the cellular and network bases of epileptic seizures. Annu. Rev. Physiol. **63**,

815–846.

[34] Merz P., Freisleben B., 1999. Fitness landscapes and memetic algorithm design. New ideas in optimization. 245–260.

[35] Milton J., Jung P., 2003. Epilepsy as a dynamic disease. Springer (Verlag).

[36] Mitchell, T., 1997. Machine Learning. McGraw Hill.

[37] Mitchell, M., 1998. An Introduction to Genetic Algorithms. MIT Press.

[38] Nashef L., Shorvon S. D., 1997. Mortality in Epilepsy. Epilepsia **38**, 1059–1061.

[39] Niedermeyer E., Lopes da Silva F. H. (eds), 2005. Electroencephalography: Basic principles, clinical applications, and related fields. Philadelphia: Lippincott Williams and Wilkins 5th edn.

[40] Nunez, P.L., 1974. The brain wave equation: a model for the EEG. Math. Biosci. **15**, 279–297.

[41] Polack, P.O., Guillemain, I., Hu, E., Deransart, C., Depaulis, A., Charpier, S., 2007. Deep Layer Somatosensory Cortical Neurons Initiate Spike-and-Wave Discharges in a Genetic Model of Absence Seizures. J. Neurosci. **27**, 6590–6599.

[42] Proposal for revised classification of epilepsies and epileptic syndromes. Commission on Classification and Terminology of the International League Against Epilepsy. Epilepsia. **30**,389–399.

[43] Pugliatti M., Behi E., Forsgren L., Ekman M., Sobocki P., 2007. Estimating the cost of epilepsy in Europe: A review with economic modeling. Epilepsia **48**, 2224–2233.

[44] Robinson, P.A., Rennie, C.J., Wright, J.J., 1997. Propagation and stability of waves of electrical activity in the cerebral cortex. Phys. Rev. E **56**, 826–840.

[45] Robinson, P.A., Rennie, C.J., Rowe, D.L., 2002. Dynamics of large-scale brain activity in normal arousal states and epileptic seizures. Phys. Rev. E **65**, 041924.

[46] Robinson, P.A., Rennie, C.J., Rowe, D.L. and O'Connor, S.C., 2004 Estimation of multiscale neurophysiologic parameters by electroencephalographic means. Hum. Brain Mapp. **23**, 53–72.

[47] Rodrigues S., Terry J. R., Breakspear M., 2006. On the genesis of spike-wave oscillations in a mean-field model of human thalamic and corticothalamic dynamics. Phys. Lett. A **355**, 352–357.

[48] Rodrigues, S., Barton, D., Marten, F., Kibuuka, M., Alarcon, G., Richardson, M.P., Terry, J.R. 2010. A method for detecting false bifurcations in dynamical systems: application to neural-field models. Biol. Cybern. **102**, 145–154.

[49] Rodrigues, S., Barton, D., Szalai, R., Benjamin, O., Richardson, M.P., Terry, J.R., 2009. Transitions to spike-wave oscillations and epileptic dynamics in a human cortico-thalamic mean-field model. J. Comp. Neurosci. **27**, 507–526.

[50] Sogawa Y., Moshé S., Shinnar S., Dlugos D., Conry J., Cnaan A., Glauser T., 2009. Petit-mal sonata: predominant EEG seizure patterns in childhood absence epilepsy (CAE). Epilepsia **50**, S10 94–95.

[51] Steriade, M., 2003. Neuronal Substrates of Sleep and Epilepsy. Cambridge University Press.

[52] Stokes T., Shaw E. J., Juarez-Garcia A., Camosso-Stefinovic J., Baker R., 2004. Clinical Guidelines and Evidence Review for the Epilepsies: diagnosis and management in adults and children in primary and secondary care. London: Royal College of General Practitioners).

[53] Suffczynski, P., Kalitzin, S., Lopes da Silva, F., 2004. Dynamics of non-convulsive epileptic phenomena modeled by a bistable neuronal network. Neurosci. **126**, 467–484.

[54] Suffczynski, P., Lopes da Silva, F., Parra, J., Velis, D., Kalitzin, S., 2005. Epileptic transitions: model predictions and experimental validation. J. Clin. Neurophysiol. **22**, 288–299.

[55] Sywerda, G., 1989. Uniform crossover in genetic algorithms. Proc. Third Int. Conf. on Genetic Algorithms.

[56] Tsiptsios D. I., Howard R. S., Koutroumanidis M. A., 2010. Electroencephalographic assessment of patients with epileptic seizures. Expert Rev Neurother. **10**, 1869–1886.

[57] Wendling, F., Hernandez, A., Bellanger, J.J., Chauvel, P., Bartolomei, F., 2005. Interictal to ictal transition in human temporal lobe epilepsy: insights from a computational model of intracerebral EEG. J. Clin. Neurophysiol. **22**, 343–356.

[58] Wilson H.R., Cowan J.D., 1972. Excitatory and inhibitory interactions in localized populations of model neurons. Biophys.

J. 12, 1–24.

[59] Yenjun S., Harvey A. S., Marini C., Newton M. R., King M. A., Berkovic S. F., 2003. EEG in adult-onset idiopathic generalized epilepsy. Epilepsia **44**, 252–256.

parameter	***type***	***fixed value/range***	***units***
γ_E	free	$[10, 200]$	s^{-1}
α	free	$[10, 200]$	s^{-1}
β	fixed ratio	3α	s^{-1}
A	free	$[0.1, 100]$	s^{-1}
B	fixed ratio	$3A$	s^{-1}
Q_{max}	fixed	250	s^{-1}
θ	fixed	0.015	V
σ	fixed	0.006	V
ν_{ee}	fixed	0.001	$V \cdot s$
ν_{ei}	fixed	-0.0018	$V \cdot s$
ν_{es}	fixed	0.0017	$V \cdot s$
ν_{re}	fixed	$5e-005$	$V \cdot s$
ν_{rs}	fixed	$5e-004$	$V \cdot s$
ν_{sn}	fixed	0.004	$V \cdot s$
ν_{sr}	fixed	$-8e-004$	$V \cdot s$
ν_{srB}	fixed	$-8e-004$	$V \cdot s$
ν_{se}	fixed	0.003	$V \cdot s$

Table 1: Table showing the list of parameters of our model and in the cased of those parameters ultimately fixed, the values to which they were assigned. The term "fixed ratio" is used if their value is proportional to a free parameter.

Figure Legends

Figure 1. Exemplar spike-wave discharges. Two separate spike and wave discharges (upper and lower panels), recorded from the same patient. The red dashed boxes illustrate similarly evolving features across each discharge. The recordings are taken from electrode placing O2, using a standard 10-20 system.

Figure 2. Schematic of the model. (a) Schematic of our modelling framework, representing three neural masses (e, r, s) which are the main components of the thalamocortical loop. The lines represent connections between the different masses, with arrowheads representing excitatory synaptic connections, whilst circles are inhibitory connections. (b) Example of the variation of the model dynamics as presented in [32]. We consider the bifurcation plane in two-parameter space: ν_{se} and $\tau_{gaba} \equiv 4/3A$. The dotted curves define bifurcations which correspond to boundaries of different periodic solutions of the model. The black curves divide the plane into distinct regions, corresponding to different spike and wave profiles. The colours corresponding to the number of spikes occurring in a single cycle. The legend depicts a single cycle for each case.

Figure 3. Interpretation of EEG dynamics. Sketch describing three ways to interpret EEG dynamics for separate times $t1 < t2 < t3$ during a spike and wave discharge. In panel (a) the evolution of activity arises as a result of a stable attractor which continuously changes shape, due to slow changes in underlying system parameters as time progresses. In panel (b) evolution of the EEG waveform is accounted for by following a (noisy) transient path around a stable attractor (i.e. there is no need for variation of underlying system parameters). In panel (c) evolution of the EEG waveform results from following a transient around a slowly evolving attractor (i.e. a combination of (a) and (b).

Figure 4. Schematic of the algorithm. Schematic of the successive steps within the algorithm for obtaining the path through parameter space from patient EEG. The whole process consists of 6 stages, which starts with a clinical EEG recording and ends with a path through parameter space. The specific details of each of these stages is described in the methods section.

Figure 5. Filtering methods. Panel (a1) shows a two second window of EEG during a spike and wave discharge from our database, with the sharp spikes highlighted in red. (a2) The same data after application of a digital second order Butterworth filter, with $f_c = 30$Hz. (b1) A two second window of output of the model. (b2) Model output after application of the second order continuous Butterworth filter with $f_c = 30$Hz. (c-d) Frequency response comparing continuous (blue line) and digital (red line) second order Butterworth filters. The dashed line marks the cutoff frequency f_c.

Figure 6. Periodicity functions for experimental and simulation data. Column (a): segmentation procedure applied to an exemplar EEG signal. Column (b): segmentation procedure applied to an exemplar output from the model. In both figures, the upper panel shows the original signal. The central panels show the corresponding periodicity function $p(\tau)$, where a dashed line and a circle denotes the value of τ which

corresponds to the approximate period T of the original signal. The lower panel shows the original signal, superimposed with the same signal filtered with a narrow band pass filter around frequency 1/T (grey line). The dashed lines show the cutting points calculated for this signal.

Figure 7. Finite state machine used for feature detection. (a) Following conventions, circles represent states while arrows state transitions. Also following conventions, the input/operation relationship is attached to the arrow of the corresponding transition. (b) Two examples of execution of the finite state machine for two different signals. The upper signal is an hypothetical EEG signal without noise or artifacts, while the lower one is the same signal after the addition of Gaussian noise.

Figure 8. Descriptive diagram of the genetic algorithm used to estimate model parameters. The four phases are represented as light grey boxes, which include sub-diagrams of the successive operations within each phase. The smaller vertical rectangles represent chromosomes, whose shade of grey indicates their value of error. If this error has not been calculated at a specific stage, it is labelled with a question mark. Chromosomes always appear grouped in a common row, representing different sets that are handled by the algorithm. Legends beside each row provide the set name and its general description. The four thick grey arrows represent the general flow of the algorithm from one phase to the next, while thin black arrows represent smaller operands performed on the chromosomes during each phase. Legends beside each thin arrow give a general description of the performed operation.

Figure 9. Clustering and parameter trends. Illustrating how cluster and subsequently parameter evolutions are obtained from the output of the genetic algorithm. In the case where there is multiple cluster centres per cycle (for example due to bistability of the model), we select the one with the lowest average error function. The centre of this cluster (red circle) is then projected into three parameter space, and its evolution is smoothed by an exponential filter (solid light red curve).

Figure 10. EEG features eliminated by measurement noise. An example of how EEG features may be eliminated as a consequence of measurement noise. (a) A hypothetical EEG signal with no noise. Panel (b) shows how noise could manipulate the signal. For example, in the middle spike wave cycle, the noise has destroyed two major features; a spike and an inflection point, which are marked by the left and right black circles respectively. In both cases the grey line represents the EEG, while black points represent the same (time sampled) signal without noise.

Figure 11. Method of testing and validation using pseudo-data. (a) The upper panels show an artificially generated spike wave cycle with increased levels of additive gaussian noise (black line), together with an example of ϕ_{eF} calculated by the genetic algorithm (grey line). The lower panels show the parameters of 88 fits to each artificial cycle in the corresponding upper panel (grey stars). Also included are the calculated cluster centres (blue circles); the centre that is representative for each artificial cycle (red circle); and the original parameters that generated the artificial cycle (black dot). (b) Comparison of a parameter path used to generate a series of 12 artificial cycles (light brown), and the path through 12 centres of representative

clusters, after executing the whole algorithm (dark brown); a noise level of 5% was used. (c) The upper figure shows the series of 12 artificial cycles used in (b), while the lower figure shows an exemplar fit of ϕ_{eF} to each cycle. The light grey background shows the area of the signal where the algorithm is not scanning for features.

Figure 12. Bifurcation plane analysis of parameter estimates. (a) Three dimensional view of the 20% fits with lowest error in 440 fits per spike-wave cycle, using all the cycles from our database (grey stars). Note that most of them line up within a two dimensional structure, which is approximated by a two-dimensional bifurcation plane. Panel (b) considers this bifurcation plane, displaying various regions of periodic model solutions. The different types of solutions are colour coded as per the legend. (c1,c2) Two examples of spike wave cycles from our database (black curves) and an exampler fitted model solution (grey curves). Panels (d1,d2) display the parameters of the 20% fits with lowest error in 440 fits per cycle, using the cycles of (c1) and (c2) respectively (grey stars). They are shown projected onto the bifurcation diagram in γ_e and α.

Figure 13. Comparison of fitted model output to EEG data. llustrating the model output for the best parameter estimates (ϕ_{eF}) to a series of EEG-cycles $g_{F,k}$, which are taken from the spike-wave discharge of the second seizure in Patient C.

Figure 14. Path through parameter space. The path through parameter space obtained by the fitting the model to spike-wave discharges from six discharges (three patients A,B,C and two discharges per patient). Panels (a,b,c) show the evolution in each patient. The textbox shows the clinical metadata for each patient.

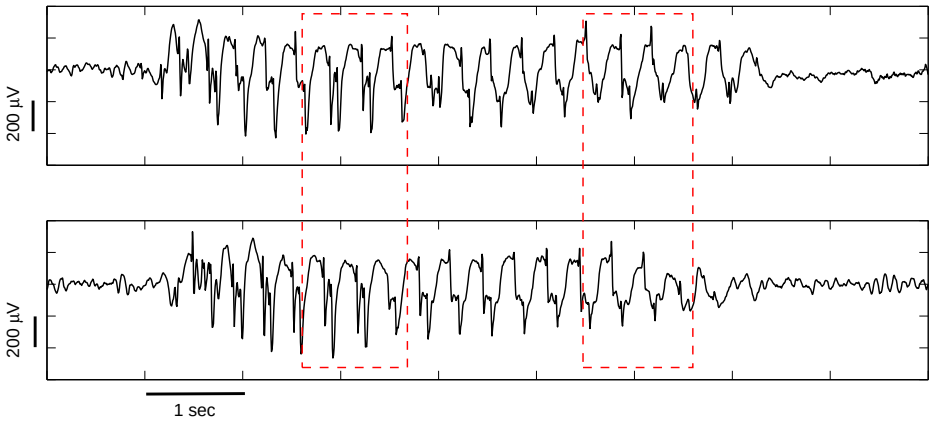

Figure 1:

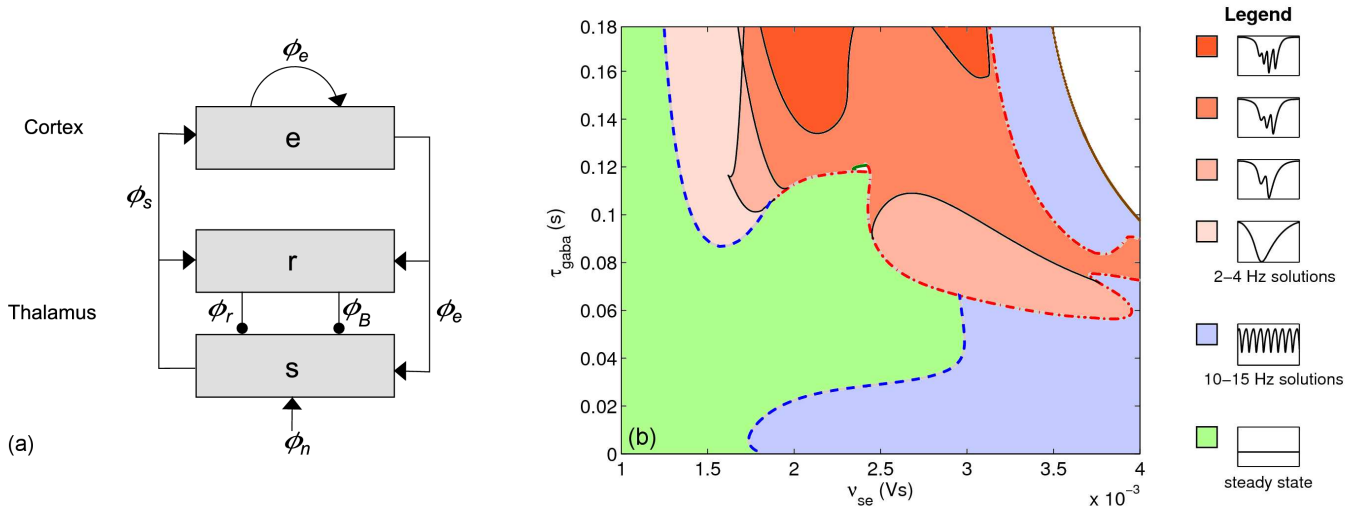
Cortex
Thalamus
e
r
s
(a)
(b)
Legend
2–4 Hz solutions
10–15 Hz solutions
steady state
x 10^-3

Figure 2:

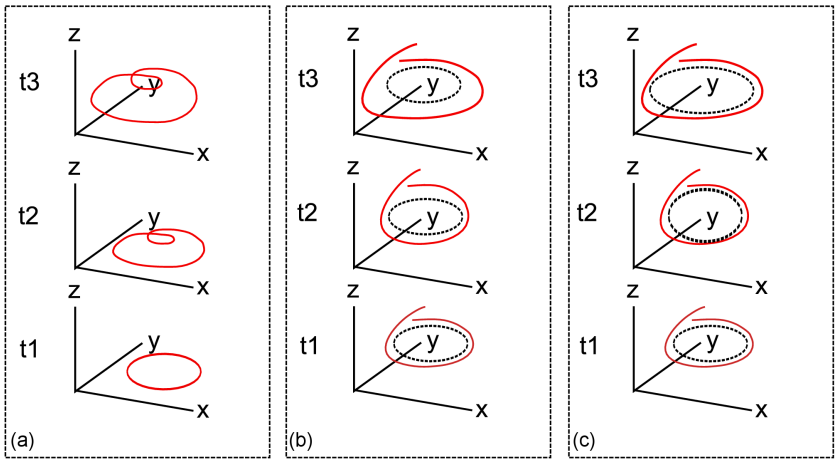

Figure 3:

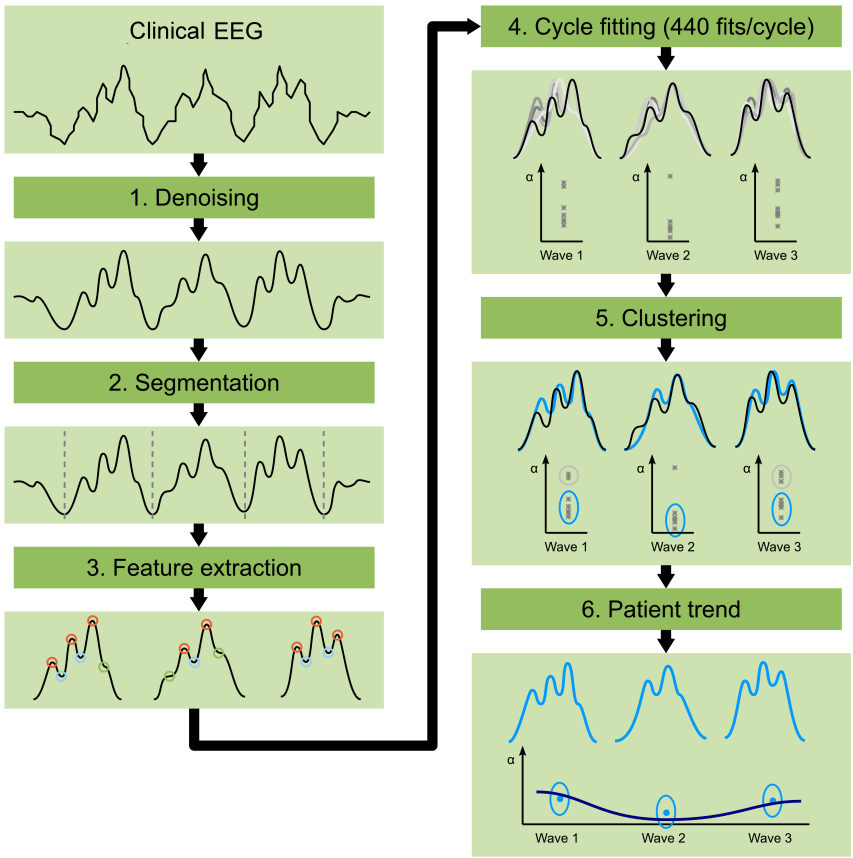
Clinical EEG
1. Denoising
2. Segmentation
3. Feature extraction
4. Cycle fitting (440 fits/cycle)
α
Wave 1
Wave 2
Wave 3
5. Clustering
6. Patient trend

Figure 4:

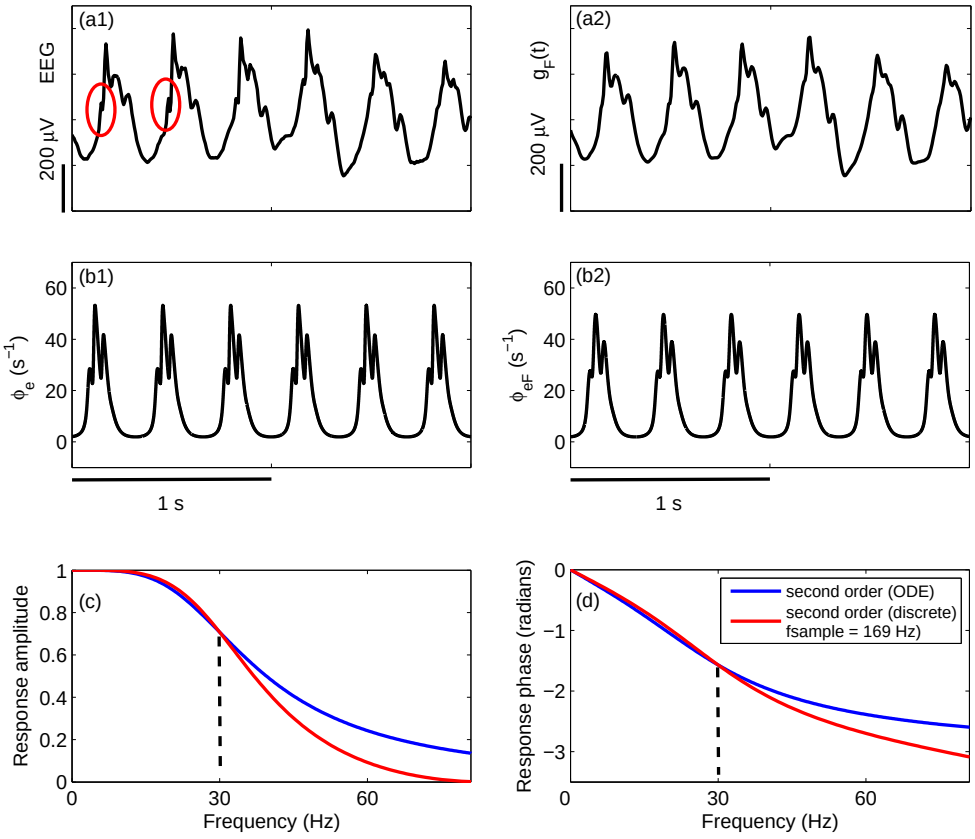
(a1)
EEG
200 μV
(a2)
$g_F(t)$
200 μV
(b1)
ϕ_e (s^{-1})
60
40
20
0
1 s
(b2)
ϕ_{eF} (s^{-1})
60
40
20
0
1 s
(c)
Response amplitude
1
0.8
0.6
0.4
0.2
0
0
30
60
Frequency (Hz)
(d)
Response phase (radians)
0
−1
−2
−3
0
30
60
Frequency (Hz)
second order (ODE)
second order (discrete)
fsample = 169 Hz)

Figure 5:

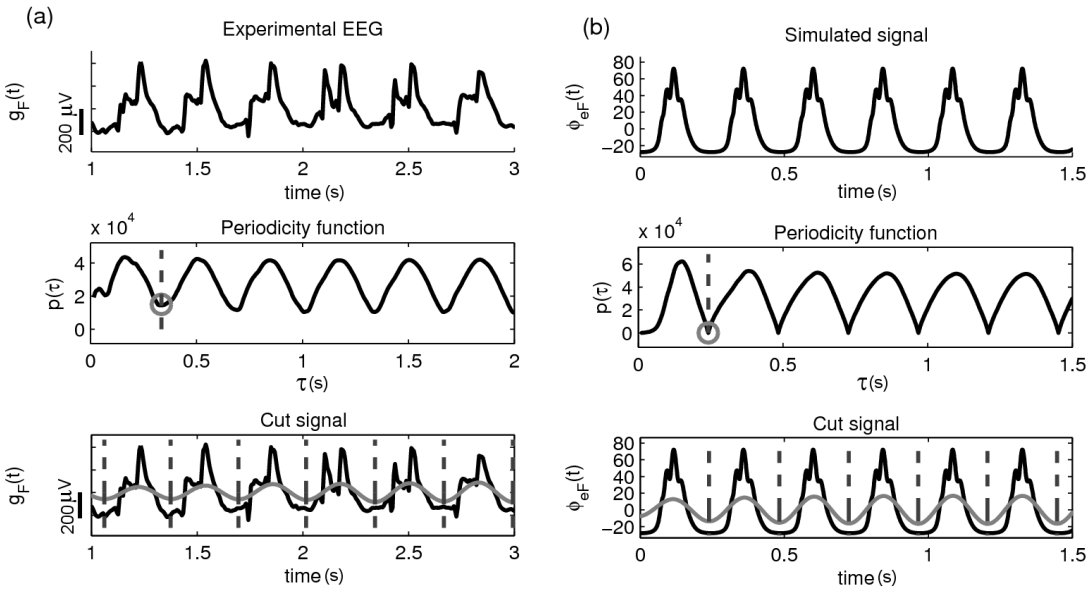
(a)
Experimental EEG
$g_F(t)$
200 µV
time (s)
x 10^4
Periodicity function
p(τ)
τ(s)
Cut signal
$g_F(t)$
200µV
time (s)
(b)
Simulated signal
$\phi_{eF}(t)$
time (s)
x 10^4
Periodicity function
p(τ)
τ(s)
Cut signal
$\phi_{eF}(t)$
time (s)

Figure 6:

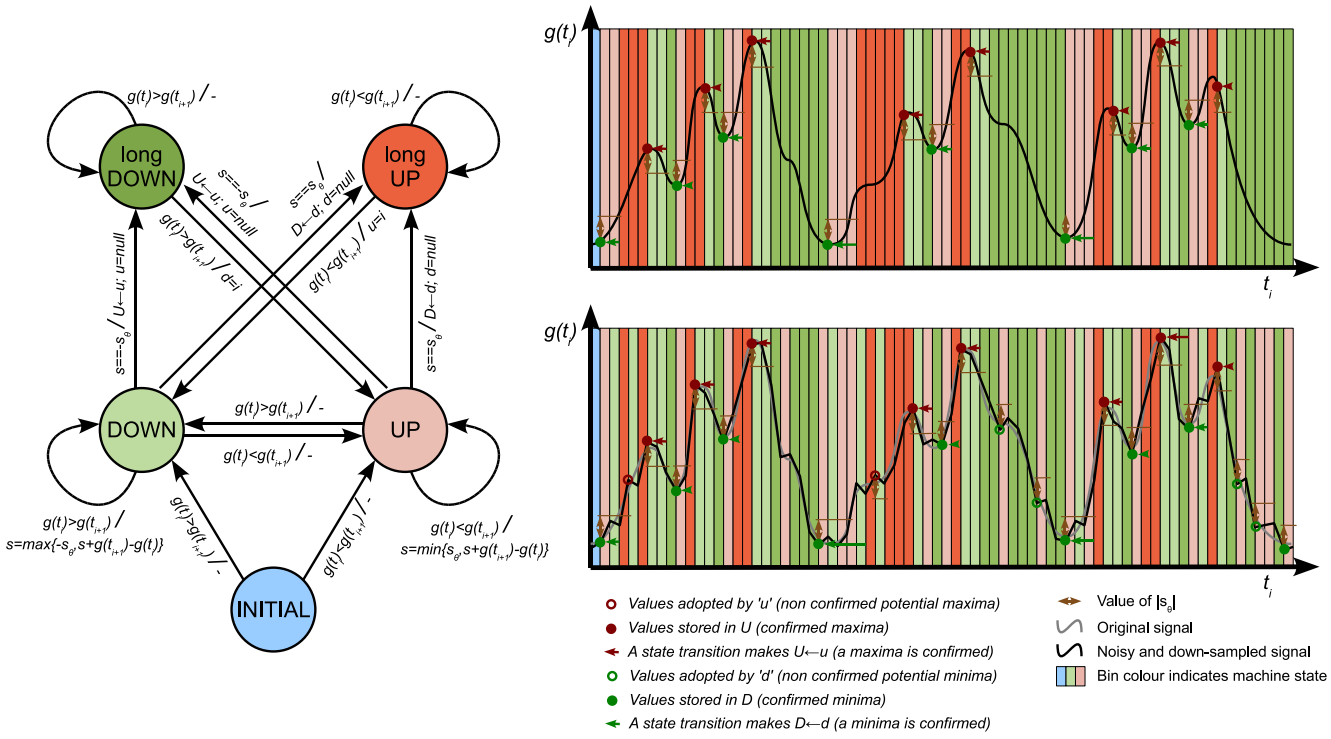
long DOWN
long UP
DOWN
UP
INITIAL
g(t_i)>g(t_i+1) / -
g(t_i)<g(t_i+1) / -
s==-s_θ / U←u; u=null
s==s_θ / D←d; d=null
g(t_i)>g(t_i+1) / d=i
g(t_i)<g(t_i+1) / u=i
g(t_i)>g(t_i+1) / s=max{-s_θ, s+g(t_i+1)-g(t_i)}
g(t_i)<g(t_i+1) / s=min{s_θ, s+g(t_i+1)-g(t_i)}
g(t_i)
t_i
Values adopted by 'u' (non confirmed potential maxima)
Values stored in U (confirmed maxima)
A state transition makes U←u (a maxima is confirmed)
Values adopted by 'd' (non confirmed potential minima)
Values stored in D (confirmed minima)
A state transition makes D←d (a minima is confirmed)
Value of |s_θ|
Original signal
Noisy and down-sampled signal
Bin colour indicates machine state

Figure 7:

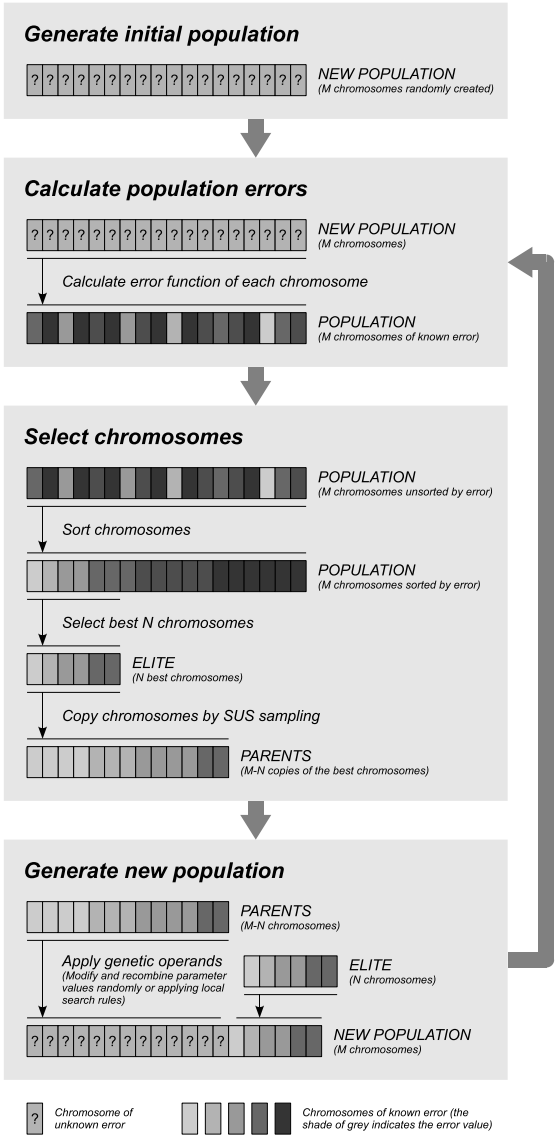
Generate initial population
NEW POPULATION
(M chromosomes randomly created)
Calculate population errors
NEW POPULATION
(M chromosomes)
Calculate error function of each chromosome
POPULATION
(M chromosomes of known error)
Select chromosomes
POPULATION
(M chromosomes unsorted by error)
Sort chromosomes
POPULATION
(M chromosomes sorted by error)
Select best N chromosomes
ELITE
(N best chromosomes)
Copy chromosomes by SUS sampling
PARENTS
(M-N copies of the best chromosomes)
Generate new population
PARENTS
(M-N chromosomes)
Apply genetic operands
(Modify and recombine parameter values randomly or applying local search rules)
ELITE
(N chromosomes)
NEW POPULATION
(M chromosomes)
Chromosome of unknown error
Chromosomes of known error (the shade of grey indicates the error value)

Figure 8:

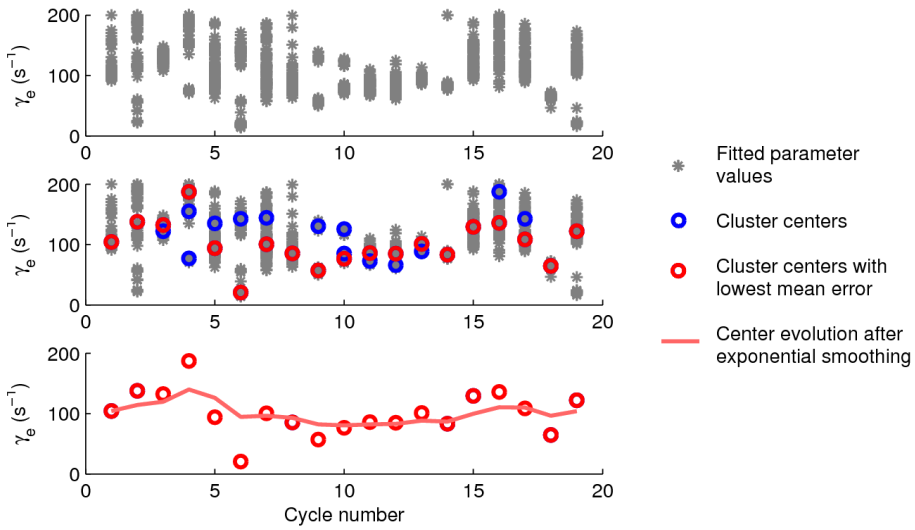
200
100
0
γ_e (s^{-1})
0
5
10
15
20
Cycle number
Fitted parameter values
Cluster centers
Cluster centers with lowest mean error
Center evolution after exponential smoothing

Figure 9:

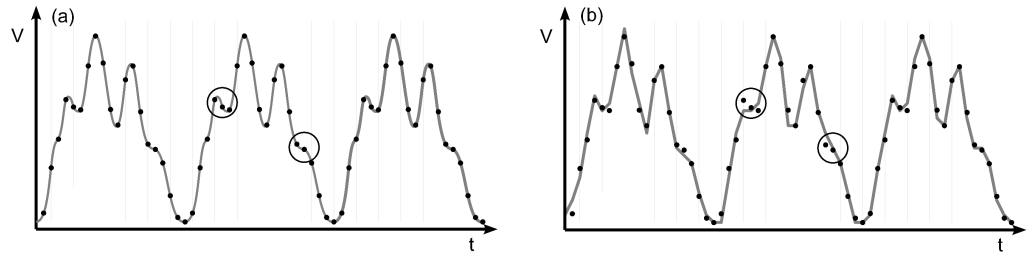

Figure 10:

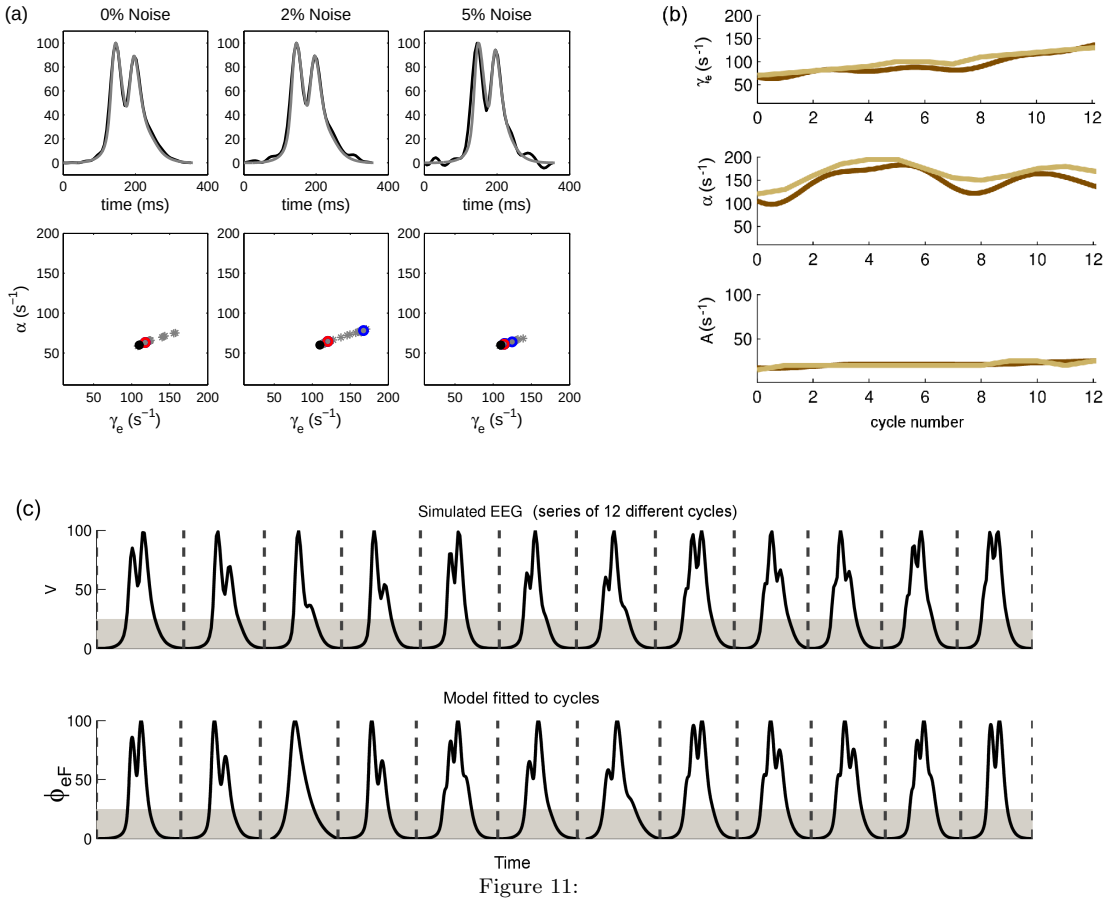
(a)
0% Noise
2% Noise
5% Noise
time (ms)
α (s⁻¹)
γe (s⁻¹)
(b)
γe (s⁻¹)
α (s⁻¹)
A(s⁻¹)
cycle number
(c)
Simulated EEG (series of 12 different cycles)
V
Model fitted to cycles
ϕeF
Time

Figure 11:

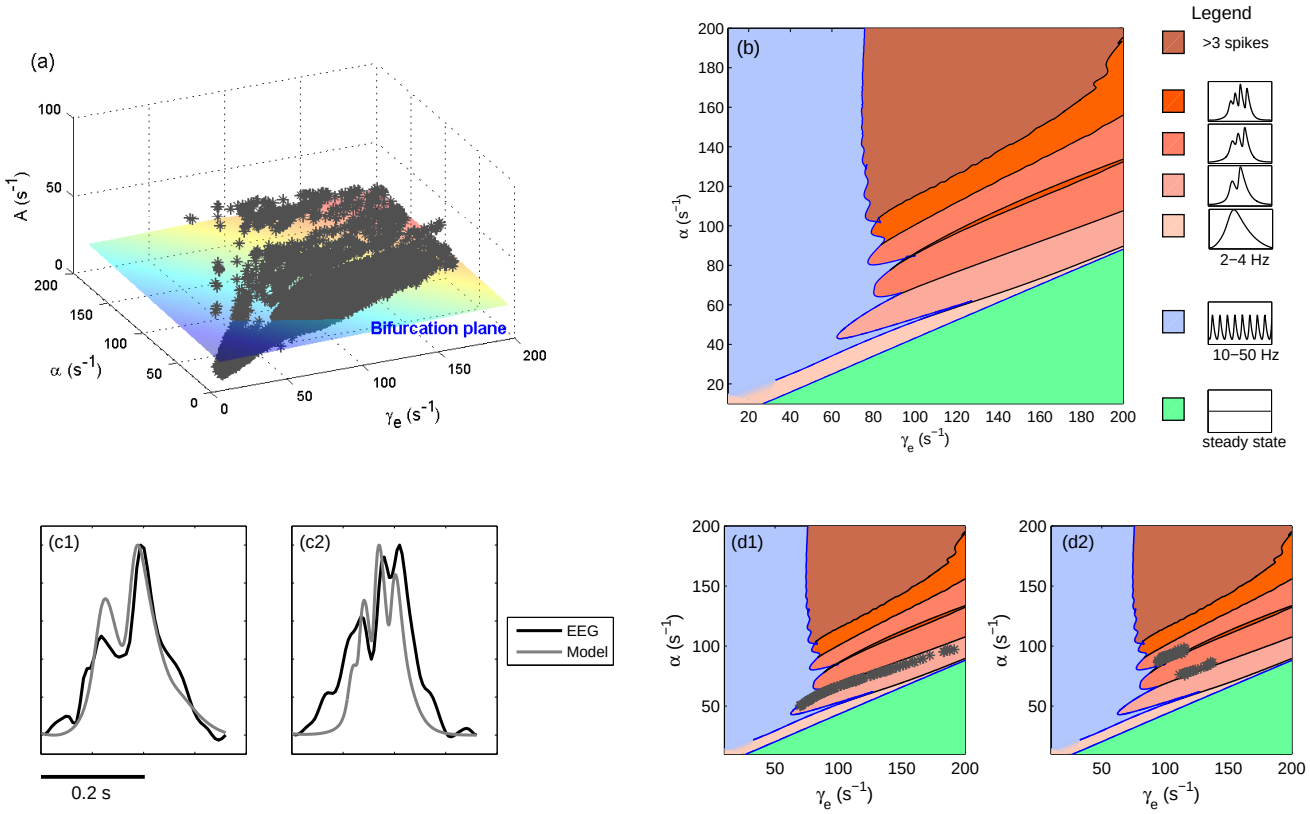
(a)
A (s^{-1})
α (s^{-1})
γe (s^{-1})
Bifurcation plane
(b)
α (s^{-1})
γe (s^{-1})
Legend
>3 spikes
2–4 Hz
10–50 Hz
steady state
(c1)
(c2)
EEG
Model
0.2 s
(d1)
(d2)

Figure 12:

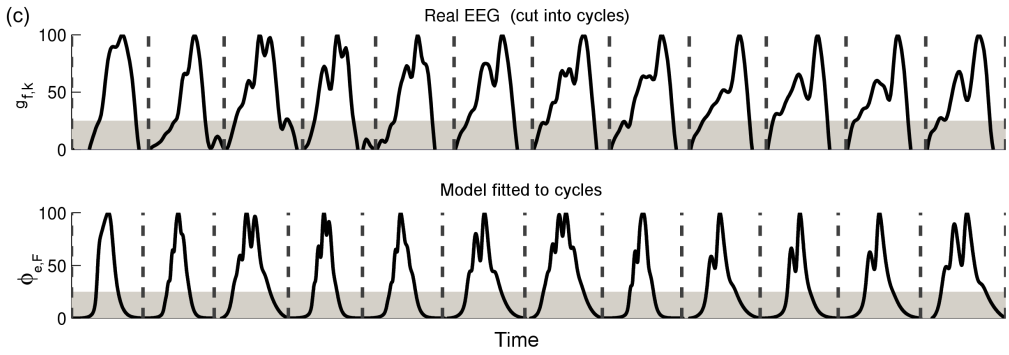
(c)
Real EEG (cut into cycles)
100
50
0
$g_{f,k}$
Model fitted to cycles
100
50
0
$\phi_{e,F}$
Time

Figure 13:

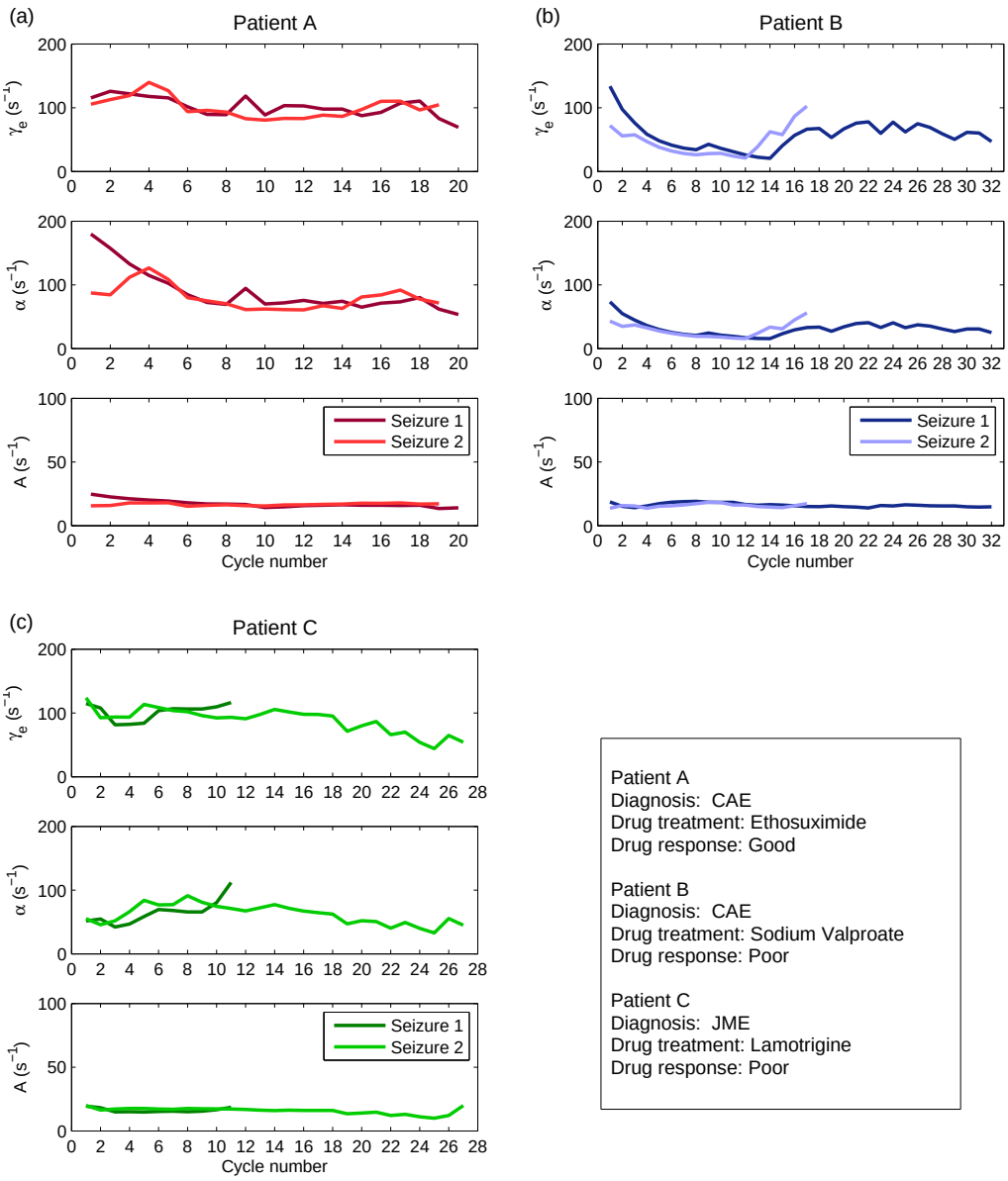

Patient A
Diagnosis: CAE
Drug treatment: Ethosuximide
Drug response: Good

Patient B
Diagnosis: CAE
Drug treatment: Sodium Valproate
Drug response: Poor

Patient C
Diagnosis: JME
Drug treatment: Lamotrigine
Drug response: Poor

Figure 14: